The Astrophysical Journal, 890:66 (16pp), 2020 February 10 https://doi.org/10.3847/1538-4357/ab67be

Are Faint Supernovae Responsible for Carbon-enhanced Metal-poor Stars?

Yutaka Komiya[1], Takuma Suda[1,2,5], Shimako Yamada[3], and Masayuki Y. Fujimoto[3,4]
[1] Research Center for the Early Universe, University of Tokyo, Hongo 7-3-1, Bunkyo-ku, 113-0033, Tokyo, Japan
[2] Open University of Japan, Wakaba 2-11, Mihama-ku, 261-8586, Chiba, Japan
[3] Graduate School of Science, Hokkaido University, Kita 6 Nishi 10, Kita-ku, Sapporo 060-0810, Japan
[4] Faculty of Engineering, Hokkai-Gakuen University, Asahimachi 4-1-40, Toyohira-ku, Sapporo 060-0810, Japan
Received 2019 September 14; revised 2019 December 24; accepted 2020 January 3; published 2020 February 12

Abstract

Mixing and fallback models in faint supernova models are supposed to reproduce the abundance patterns of observed carbon-enhanced metal-poor (CEMP) stars in the Galactic halo. A fine-tuning of the model parameters for individual stars is required to reproduce the observed ratios of carbon to iron. We focus on extremely metal-poor stars formed out of the ejecta from the mixing and fallback models using a chemical evolution model. Our chemical evolution models take into account the contribution of individual stars to chemical enrichment in host halos, together with their evolution in the context of the hierarchical clustering. Parameterized models of mixing and fallback models for Population III faint supernovae are implemented in the chemical evolution models with merger trees to reproduce the observed CEMP stars. A variety of choices for model parameters on star formation and metal pollution by faint supernovae are unable to reproduce the observed stars with $[Fe/H] \lesssim -4$ and $[C/H] \gtrsim -2$, which are the majority of CEMP stars among the lowest-metallicity stars. Only possible solution is to form stars from small ejecta mass, which produces an inconsistent metallicity distribution function. We conclude that not all the CEMP stars are explicable by the mixing and fallback models. We also tested the contribution of binary mass transfers from AGB stars that are also supposed to reproduce the abundances of known CEMP stars. This model reasonably reproduces the distribution of carbon and iron abundances simultaneously only if we assume that long-period binaries are favored at $[Fe/H] \lesssim -3.5$.

Unified Astronomy Thesaurus concepts: Galaxy chemical evolution (580); Chemical enrichment (225); Halo stars (699); Population II stars (1284); Population III stars (1285)

1. Introduction

Extremely metal-poor (EMP) stars in the Milky Way (MW) halo are the survivors of the very early generations of stars. They are interesting objects as a key to the understanding of the formation, evolution, and explosion of first stars, as well as of the early phases of galaxy formation and chemical evolution.

The most prominent feature of EMP stars is a high frequency of carbon-enhanced stars that are classified as carbon-enhanced metal-poor (CEMP) stars (e.g., Beers & Christlieb 2005). The well-accepted criterion of CEMP stars is $[C/Fe] > 0.7$ (Aoki et al. 2007). CEMP stars occupy 20%–30% of EMP stars (Rossi et al. 1999; Carollo et al. 2014; Lee et al. 2014).

The percentage of carbon-enhanced stars is higher at lower metallicity. Among 27 ultra–metal-poor (UMP) stars with $[Fe/H] < -4$, registered in the SAGA database that compiles the published observational data of EMP stars (Suda et al. 2008, 2011, 2017; Yamada et al. 2013), 17 stars have carbon abundance with $[C/Fe] > 0.7$ in the 2018 April 11 version. Furthermore, in the case of five hyper–metal-poor (HMP) stars with $[Fe/H] < -5$, all of them show large carbon enhancement. All of the HMP stars and most of the UMP stars have a carbon abundance of $-1 \gtrsim [C/H] \gtrsim -2.5$, as shown in Figure 1. We refer to these stars together as carbon-rich UMP (CRUMP) stars in this paper.

It is known that the majority of CEMP stars also show the enhancement of *s*-process elements (e.g., Aoki et al. 2007). These stars are called CEMP-*s* stars (the definition is $[Ba/Fe] > 0.5$ in this paper), while stars without the enhancement of *s*-process elements are referred to as CEMP-no stars.

Yoon et al. (2016) proposed another classification of CEMP stars according to the carbon and iron abundances. They divided CEMP stars into three groups. The Group I stars are those with large carbon abundances ($[C/H] \gtrsim -1.3$) in the metallicity range of $[Fe/H] \simeq -4$ to -2. The vast majority of the Group I stars are CEMP-*s* stars, but a dozen CEMP-no stars are also classified into Group I. The Group II population consists of stars with small C enhancement ($[C/Fe] \lesssim +1$) at extremely low metallicity ($[Fe/H] \simeq -5.0$ to -2.5). They are all members of CEMP-no stars. Stars with significant C enhancement with $[C/H] \simeq -1$ to -2 and in the lowest metallicity range ($[Fe/H] \lesssim -3.5$) are classified into Group III. They are almost overlapped with CRUMP stars and are classified as CEMP-no stars, although most of them have measured Ba abundances with only loose upper limits at $[Ba/Fe] > 0.5$.

It is now widely accepted that CEMP-*s* stars are formed through binary mass transfer from intermediate-mass companion stars. Intermediate-mass stars produce carbon and *s*-process elements and dredge them up in the surface during the TP-AGB phase, though the enhancement of *s*-process elements depends on their progenitor mass (e.g., S. Yamada et al. 2020a, in preparation). After mass transfer events via stellar wind or the Roche lobe overflow, the secondary companion becomes carbon- and *s*-process-enhanced stars. These secondary stars should be observed as CEMP stars with extinct white dwarf companions. Observationally, radial velocity variations were detected for most of the CEMP-*s* stars that were subject to the monitoring of their radial velocities (Lucatello et al. 2005; Starkenburg et al. 2014).

On the other hand, the comprehensive scenario for the origin of CEMP stars including CEMP-no and CRUMP stars is not

[5] Corresponding author.

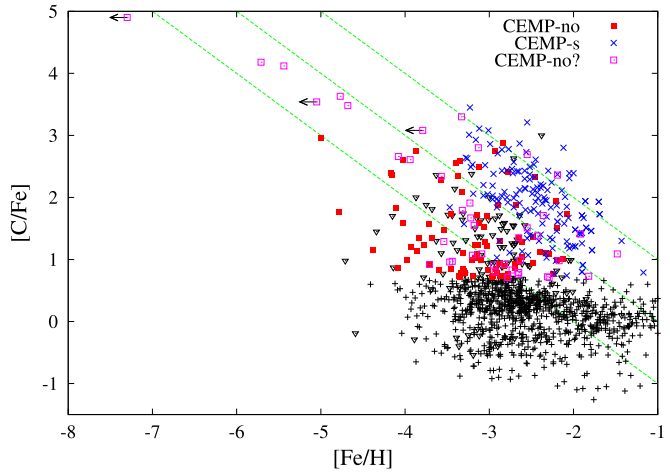

Figure 1. Distribution of the metal-poor stars on the metallicity ([Fe/H]) and the carbon enhancement ([C/Fe]) diagram, where CEMP-*s* stars (blue crosses), CEMP-no stars (red filled squares), and carbon-normal stars (black plus signs) are plotted. Stars with upper limits for carbon abundances are plotted with the inverted triangles. Magenta open squares denote CEMP stars with upper limits for barium enhancement having [Ba/Fe] > 0.5, or CEMP stars without the measurement of barium abundances. Horizontal arrows stand for upper limits for iron abundances. Dashed green diagonal lines are the constant values of [C/H] $= 0, -1, -2$ from top to bottom. The observational data are taken from the SAGA database (http://sagadatabase.jp/).

yet established. So far, three major scenarios have been proposed, all of which tried to explain the origin of CRUMP stars (in particular, HE 0107–5240), while they are applicable to other CEMP-no stars.

The first scenario considers peculiar supernovae (SNe) that eject high-[C/Fe] material. If a star explodes as a core-collapse SN (CCSN), its ejecta will have large [C/Fe] supposing that iron-rich material at their inner region falls back onto the central compact object while carbon-rich material at the outer layer is blown off. If the first SN was a "faint SN" and contains a small amount of iron in the yields, the second-generation stars, formed out of these carbon-enhanced ejecta, will be CEMP-no or CRUMP stars.

The "mixing and fallback" model associated with faint SNe was proposed by Umeda & Nomoto (2005b). They assume that the matter in the mass coordinate between $M_{\rm cut}$ and $M_{\rm mix}$ is mixed at the explosion phase and that a certain fraction, $f_{\rm fb}$, of the mixed region is ejected, whereas the rest of the mixed material falls back onto a black hole. They reproduced the abundance pattern of an HMP star, HE 0107–5240, using this model. The abundance patterns of other CEMP stars are also explained by employing other parameters for the mixing and fallback (Iwamoto et al. 2005; Umeda & Nomoto 2005a; Tominaga et al. 2013).

The second scenario is the binary scenario (Suda et al. 2004; Komiya et al. 2007), where binary mass transfer plays a role in the formation of CEMP-no stars as it does for CEMP-*s* stars. In the standard framework of the stellar evolution without extra mixing processes, EMP stars in the mass range of $\sim$0.8–3.5 $M_\odot$ undergo helium-flash-driven deep mixing (He-FDDM), which is triggered by the hydrogen engulfment by the helium flash convection, leading to the dredge-up of carbon and *s*-process elements to their surface. For stars with $\gtrsim$3.5 $M_\odot$, He-FDDM does not take place. The *s*-process nucleosynthesis in these stars depends on other sources of neutrons such as ^{22}Ne burning. In any case, *s*-process is not efficient and should be weakly enhanced even if carbon is dredged up by the third dredge-ups. The secondaries of these stars are expected to be CEMP-no stars through binary mass transfer events. S. Yamada et al. (2020b, in preparation) point out that secondary stars with lower-mass ($\lesssim$3.5 $M_\odot$) primaries with wider separations also have a chance to be CEMP-no stars because barium abundance will not exceed [Ba/Fe] $= 0.5$ by a small amount of mass accretion.

One of the criticisms for the binary scenario is on the fraction of stars with radial velocity variations among CEMP-no stars. Starkenburg et al. (2014) argue that the fraction of confirmed binarity is not significantly higher for CEMP-no stars than the fraction for stars without carbon enhancement. However, a small amount of wind mass transfer in a wide binary with a period of $\sim$10,000 days or even larger is enough to enrich the secondary star to [C/Fe] > 0.7, where the variations of radial velocities should be difficult to detect. Hansen et al. (2016) reported binarity for three CEMP-no stars, all of which belong to Group I. Their estimated binary periods fall in the same range as CEMP-*s* stars, which is consistent with the expectation that the Group II and Group III stars belong to long-period binaries. Indeed, one of the Group III stars, HE 0107–5240, was reported to have a companion star whose binary period is longer than 10,000 days (Arentsen et al. 2019). We also note that some CEMP-no stars also show Eu/Ba ratio predicted by the *s*-process nucleosynthesis, and that the distribution of [Ba/Fe] of CEMP-no stars is different from that of C-normal EMP stars (S. Yamada et al. 2020b, in preparation).

The third scenario is the so-called "spinstar" scenario (Meynet et al. 2006; Maeder et al. 2015). In a fast-rotating metal-poor massive star, rotation-induced mixing takes place and enriches their surface with carbon and other light elements. The gas polluted by the carbon-enhanced wind from spinstars can be a progenitor of CEMP-no and CRUMP stars.

All three processes are asserted to produce carbon and other elements enhanced in CRUMP stars. However, the holistic distribution of the absolute abundances such as [C/H] and [Fe/H] for CEMP stars is not well studied.

In particular, there is a challenge to the faint-SN scenario in terms of the formation of the subsequent star formation. The mass of carbon from a faint SN should be comparable to a normal SN ($\Delta M_{\rm C} \sim 0.2\ M_\odot$), to obtain a large value of [C/Fe] from the small amount of ejected iron due to the large fraction of the fallback of the inner ejecta. If we assume that the carbon with mass $\Delta M_{\rm C}$ ejected by a first-generation SN is homogeneously mixed in the SN remnant of mass $M_{\rm sw}$, the carbon abundance will be estimated as follows:

$$[{\rm C/H}] = -2.5 + \log\left[\left(\frac{\Delta M_{\rm C}}{0.1\ M_\odot}\right)\left(\frac{M_{\rm sw}}{10^4\ M_\odot}\right)^{-1}\right]. \quad (1)$$

This estimate indicates that the typical carbon abundance of second-generation stars with a faint SN progenitor is lower than the carbon abundances of CRUMP stars with [C/H] $\gtrsim -2$. If we assume that the SN ejecta is mixed in a minihalo with $\sim 10^5\ M_\odot$, the second-generation stars of a normal SN progenitor will be born as EMP stars with [Fe/H] $\simeq -4$ to -3 and hence with [C/H] $\simeq -4$ to -3. For the case of faint SNe, they should produce the second-generation stars in the similar range of [C/H] $\simeq -4$ to -3 since $\Delta M_{\rm C}$ is comparable to that of normal SNe.

On the other hand, there is a challenge to the binary scenario and spinstar scenario on the origin of iron in CEMP-no stars. The binary mass transfer from AGB stars and wind from

spinstars leave iron mostly untouched, while carbon is enhanced. For CEMP-no stars with [Fe/H] $\gtrsim -4$, the normal SNe can be the suppliers of iron. On the other hand, we need the explanation for the extremely low iron abundance in CRUMP stars. One possible scenario for a small amount of iron in CRUMP stars is the surface pollution after their birth (Shigeyama et al. 2003; Suda et al. 2004; Komiya et al. 2009a). When low-mass Population III stars are formed, their surfaces can be polluted up to [Fe/H] ~ -5 by the accretion of interstellar medium (ISM), which is enriched with the metal ejecta of SNe, produced in the host minihalos. These stars are to be observed as HMP/UMP stars. Another possibility is the dilution of the ejecta from a normal SN in very large volume (Karlsson 2006; Komiya et al. 2015; Smith et al. 2015). An SN blast wave can blow out the gas from their host minihalo and enriches intergalactic medium (IGM) and other minihalos. The gas enriched with the diluted SN ejecta may form HMP/UMP stars as second-generation stars.

In this paper, we examine the faint-SN scenario in the framework of chemical evolution. We compute the chemical enrichment history of carbon and iron in the very early stages of the galaxy formation and compare with the observed EMP, UMP, and HMP stars. The binary scenario is also examined by including the accretion of C-rich matter ejected from the envelope of AGB stars. We do not consider the spinstar scenario because they are subject to large uncertainties on the diffusion of stellar wind, the formation of next-generation stars in the wind ejecta, and the final fate of spinstars after the wind mass loss.

The chemical evolution by the very early generations of stars, produced by faint SNe, has been investigated by some previous studies. Cooke & Madau (2014) modeled the enrichment of C and Fe by Population III SNe in minihalos to estimate the fraction of carbon-enhanced stars using the SN model of Heger & Woosley (2010). They only considered the abundance distribution by a single star formation event at $z = 20$ and ignored the influence of the formation history of galaxies.

Sarmento et al. (2017) performed hydrodynamic simulations with a new subgrid model to predict the distribution of chemical composition of star particles. In their model, CRUMP stars with [C/H] $\simeq -2 \sim -1$ are formed. However, they assumed that all the Population III stars have the yields taken from the best-fit model for SMSS J031300.36–670839.3 by Heger (2016). Also, their models are dependent on their subgrid model of metal mixing and are subject to uncertainties associated with the numerical scheme. Sharma et al. (2016) discussed the origin of CEMP stars using a cosmological hydrodynamical simulation. The drawback of their model is not to resolve the mass of the minihalos with $M_{\rm h} = 10^6\,M_\odot$, and the estimate of the chemical composition of EMP stars is dependent on their subgrid model. In all of the previous studies above, "star particles" do not mean individual stars but aggregations of stars. In this paper, we follow the formation and merging history of galaxies, together with the star formation history and the feedback effects in the host galaxies. We also take into account the pre-enrichment of IGM and the external enrichment of protogalaxies by the outflows driven by Population III SNe. We treat the formation and explosion of individual metal-poor stars in host galaxies and compute the chemical composition of each low-mass star that is supposed to survive in the MW halo.

This paper is organized as follows. In the next section, we describe our computational method, including new ingredients to investigate the contribution of faint SNe. In Section 3, we present the results with the faint-SN scenario and their parameter dependence. In Section 4, we consider the contribution of binaries under the binary scenario. Conclusions follow in Section 5.

2. Computational Method

We have developed a chemical evolution model with merger trees in previous studies (Komiya et al. 2009a, 2010, 2014, 2016), which we name the *StarTree* code. Here we only provide a brief summary of our code and describe what has been changed from our previous models and assumptions.

The main improvement of the *StarTree* code is the consideration of the chemical inhomogeneity of protogalaxies in order to investigate the effect of faint SNe. We adopt a stochastic chemical evolution model by SNe, which is described in Section 2.2. The assumptions related to faint SNe are described in Section 2.3.

We also updated the method of building merger trees (Section 2.1.1) and the schemes for the radiation feedback on Population III star formation (Section 2.1.2).

As mentioned above, the surface pollution of stars by ISM accretion can be important for HMP/UMP stars, but we do not consider the surface pollution in discussing the faint-SN scenario. This is because the abundance patterns of the elements up to the iron-group elements are explained by faint SNe without surface pollution for CEMP-no or CRUMP stars. Although our code can compute the surface pollution of Population III or EMP stars, we switched off the pollution subroutine in the following computations for faint SNe.

We also consider binary mass transfers as an alternative scenario for CEMP-no stars (Section 4). The assumptions about the binary mass transfer events are described in Section 4.

2.1. The StarTree Code

We build merger trees of galaxies based on the extended Press–Schechter method and follow the chemical enrichment along the trees. We refer to the baryonic components in the minihalos as protogalaxies.

We assume that the star formation rate, $\dot{M}_*$, in a protogalaxy is proportional to gas mass $M_{\rm gas}$,

$$\dot{M}_* = \epsilon_\star M_{\rm gas}, \tag{2}$$

where $\epsilon_\star$ is the star formation efficiency (SFE), depending on the mass of the host halo, and is defined by

$$\epsilon_\star = 1.2 \times 10^{-14} (M_{\rm h}/M_\odot)^{0.3}\ {\rm yr}^{-1}. \tag{3}$$

The fiducial value is chosen to reproduce the observed mass–metallicity relation for dwarf galaxies and to be consistent with the abundance distribution of *r*-process elements in EMP stars under the assumption that their sources are the ejecta of coalescing neutron star binaries (Komiya & Shigeyama 2016).

A central feature of the *StarTree* code is that all the individual Population III and EMP stars are registered. We consider each massive star and explore the properties of low-mass survivors. We randomly set the mass of each star according to the adopted initial mass function (IMF). We use the lognormal form of the IMF with the modification by the power-law tail at higher mass following Chabrier (2003).

The binary fraction is set at $f_b = 50\%$, where the masses of the primary stars are subject to the same IMF as single stars, while the masses of the secondary stars are determined by the mass ratio function. We employed the flat mass ratio distribution as in the previous studies (Komiya et al. 2007, 2009b). The peak mass, $M_{\rm md}$, of the IMF for EMP and Population III stars is set at 3 and 10 $M_\odot$, respectively, to be consistent with the fraction of known CEMP-*s* stars as discussed in our previous studies (Komiya et al. 2007; Suda et al. 2013; Komiya & Shigeyama 2016).

We also considered the gas infall onto the minihalos, the gas outflow by SN explosion, and the pre-enrichment of IGM by the gas outflow. The gas infall rate is assumed to be proportional to the dark matter infall rate given by the Press–Schechter merger tree. We computed the mass and metal outflow rates by individual SNe as a function of the SN explosion energy and the binding energy of protogalaxy (see also Section 2.2.2). We followed the evolution of the winds from protogalaxies by assuming the momentum-conserved snowplow model and considered the inhomogeneous metal enrichment in the IGM. We evaluated the distance between two protogalaxies in the merger trees, which were used to estimate the amount of pre-enrichment in newly formed protogalaxies and of external enrichment from other existent protogalaxies.

We used the same assumptions and model parameters as in Komiya & Shigeyama (2016) otherwise described here and in the following sections.

2.1.1. Merger Tree

We have updated the realizations of merger trees by replacing the method of Somerville & Kolatt (1999) with that of Parkinson et al. (2007).

It is pointed out that the Press–Schechter mass function based on the spherical collapse model overestimates the number of small halos (Zhang et al. 2008) compared with the results of *N*-body simulations and the results with the elliptical collapse model (Sheth et al. 2001; Sheth & Tormen 2002). Parkinson et al. (2007) modified the mass distribution function given by the Press–Schechter theory and presented a method to build merger trees by which the results of the *N*-body simulations are well reproduced.

The modification of the *StarTree* code resulted in the reduction in the number of the branches of merger trees. The number of the branches of the trees to produce MW mass with the mass of $M = 10^{12}\,M_\odot$ has decreased to ∼60,000 in the new model, from 200,000–300,000 in the previous models. The smaller the number of branches, the smaller the number of Population III and EMP stars, while the predicted abundance distributions in the following sections are not significantly affected, in particular after the typical masses of minihalos are $M_{\rm h} \gtrsim 10^7\,M_\odot$.

Cosmological parameters were updated to those provided by Planck Collaboration et al. (2016).

2.1.2. Suppression of Population III Star Formation by UV Radiation

Population III star formation in minihalos is thought to be suppressed by the irradiation of the Lyman–Werner (LW) photons. To account for this effect, we assumed that Population III protogalaxies with the virial temperature lower than 10^4 K do not form stars below the critical redshift $z_{\rm LW} = 20$ (Komiya & Shigeyama 2016). We have improved the prescription for the effect of the LW photos by computing the flux of the LW radiation and the suppression of star formation in a self-consistent way in each time step. This new treatment comes from our consideration that the LW radiation depends on a star formation rate and the IMF of Population III stars.

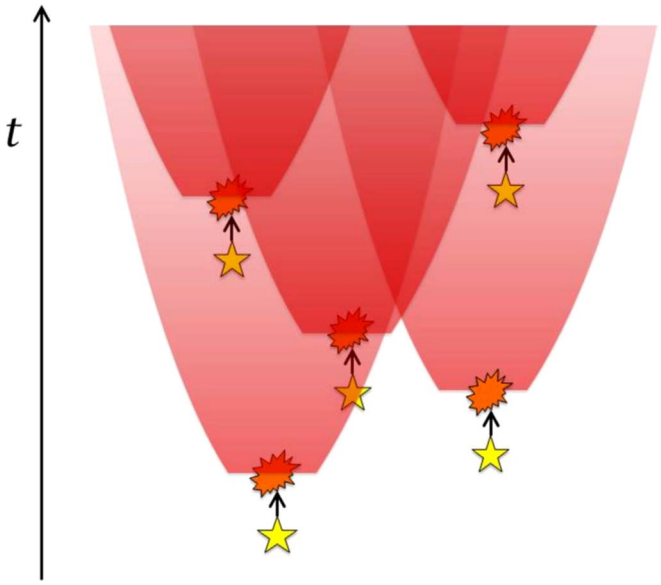

Figure 2. Schematic illustration of our stochastic chemical evolution model. The star symbols in yellow and the star polygons in red represent massive stars and the end of their lives as SNe, respectively. The red shaded areas are the ISM polluted by the yields of SNe, which expands in time by the diffusion process. The chemical enrichment of the region is affected by the sum of the pollution from SNe.

Machacek et al. (2001) provided the critical mass, $M_{\rm crit}(F_{\rm LW})$, below which the Population III minihalos do not form stars, as a function of the LW luminosity, $F_{\rm LW}$. O'Shea & Norman (2008) modified the critical mass by a factor of four based on their cosmological simulations. We adopt their formula,

$$M_{\rm crit}(F_{\rm LW}) = 4 \times \left[1.25 \times 10^5\,M_\odot + 8.7 \times 10^5\,M_\odot \left(\frac{F_{\rm LW}}{10^{-21}\ {\rm erg^{-1}\,cm^{-2}\,Hz^{-1}}}\right)^{0.47}\right]. \quad (4)$$

Using the emission rate of the LW photons from Population III stars by Schaerer (2002), we computed $F_{\rm LW}$ in each minihalo by summing up the radiations from other minihalos.

The suppression by the LW radiation works only for Population III protogalaxies and is not applied to pre-enriched protogalaxies with mass below $M_{\rm crit}$ owing to the cooling by metallic lines.

2.2. Stochastic Chemical Enrichment in a Protogalaxy

We modeled the inhomogeneous chemical evolution in a protogalaxy as a stochastic process of metal enrichment by a number of SNe. Figures 2 and 3 give schematic views on the stochastic chemical enrichment model of the minihalos. The assumptions and numerical parameters are described in the following subsections.

As shown in Figure 2, an SN explosion produces a metal-polluted region. The polluted region evolves with time by the

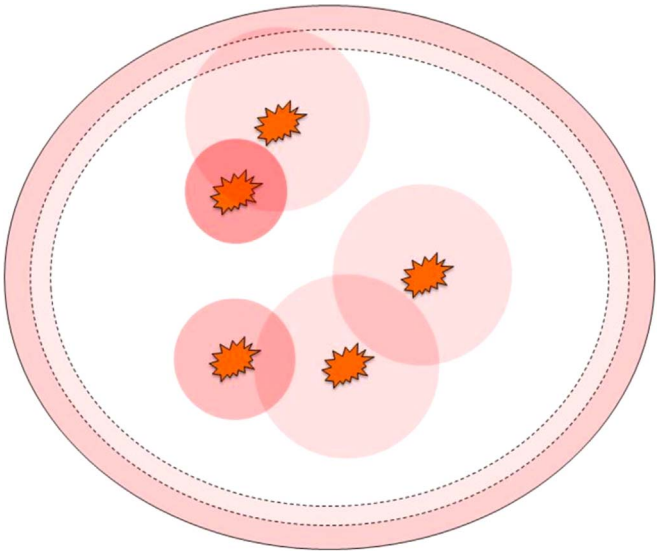

Figure 3. Schematic illustration of the metal enrichment in a protogalaxy. The star polygons in red represent the SNe in the host halo, whose boundary is shown by the ellipse in the solid line. The red shaded areas are the ISM influenced by the SN yields. The inner ring in thin red stands for the reaccretion of the outflow gas by SNe, where we assumed that the part of the ejected gas from the host halo accretes on itself again. The outer ring in dense red corresponds to infalling gas from other minihalos, which works as the pre-enrichment of the halo with metals. These rings show the initial pollution process in a simplified way. In our simulations, the accreted gas retains in the outer part of the host halo and contributes to the abundances of the subsequent generations of stars. See text for more details on the accretion and mixing of the SN yields.

diffusion process if the ejected matter remains in the host halo. The accumulation of SN yields is built up through the overwrapping of polluted regions.

Some of the outflow gas and metals, which are triggered by SNe, fall back again onto their host halos or other nearby halos, along with the infall of IGM gas. The metal abundances of the infall gas are recorded and are traced in each tree (see Section 2.2.2). The gas expelled as a galactic wind is assumed to form a spherical shell around the minihalos, i.e., the accreted gas does not mix with the host halo. The ejected gas is the source of the next-generation stars. The star formation rate is in proportion to the mass of the gas in ISM, regardless of the metallicity or the density of ISM. We do not consider the star formation triggered by the SN.

2.2.1. Metal Pollution by Each Supernova

The initial mass of the polluted region, $M_{\mathrm{p},i}$, occupied by the ith SN is given by

$$M_{\mathrm{p},i} = M_{\mathrm{sw},i} - M_{\mathrm{w},i}, \tag{5}$$

where $M_{\mathrm{sw},i}$ and $M_{\mathrm{w},i}$ denote the swept-up mass and the mass of the galactic wind (or outflow) ejected from the protogalaxy by the ith SN, respectively. The swept-up mass is prescribed as follows according to Shigeyama & Tsujimoto (1998):

$$M_{\mathrm{sw}} = 5.1 \times 10^4\, M_\odot \left(\frac{E_{\mathrm{SN}}}{10^{51}\,\mathrm{erg}}\right)^{0.97} \times \left(\frac{n_1}{1\,\mathrm{cm}^{-3}}\right)^{-0.062} \left(\frac{c_s}{10\,\mathrm{km\,s}^{-1}}\right)^{-9/7}, \tag{6}$$

where E_{SN} is the explosion energy of the SN, n_1 the number density of interstellar gas, and c_s the sound speed. The dependences on density and the sound speed are dropped for simplicity in our models. Therefore, the above equation reduces to

$$M_{\mathrm{sw}} = M_{\mathrm{sw51}} \left(\frac{E_{\mathrm{SN}}}{10^{51}\,\mathrm{erg}}\right)^{0.97}, \tag{7}$$

where $M_{\mathrm{sw51}} = 5.1 \times 10^4\, M_\odot$ is our fiducial value. We also tested a smaller value by a factor of 10, i.e., $M_{\mathrm{sw51}} = 5.1 \times 10^3\, M_\odot$. This is intended to form second-generation stars with a larger value of [C/H] from smaller swept-up mass by the first-generation SN. However, we note that the assumption of a small swept-up mass is likely to be implausible for the formation of second-generation stars. First, as seen from Equation (6), the weak density dependence of swept-up mass does not allow us to assume high density in the ISM. Second, it is also difficult to assume large sound speed in the host halo because the fiducial value of $c_s = 10\,\mathrm{km\,s}^{-1}$ corresponds to $T = 10^4\,\mathrm{K}$ and is comparable to the escape velocity of minihalos hosting Population III stars. The assumption of a larger value for c_s is unrealistic in terms of star formation.

The ejected mass by the galactic wind, M_{w}, is taken from the prescription in Komiya et al. (2014) as a function of E_{SN} and the binding energy, E_{bin}, of the protogalaxy. The energy and the mass load of the galactic wind are given by the following interpolation formulae:

$$E_{\mathrm{w}} = \eta E_{\mathrm{SN}} \left(\frac{\epsilon + \eta E_{\mathrm{SN}}/E_{\mathrm{bin}}}{1 + \eta E_{\mathrm{SN}}/E_{\mathrm{bin}}}\right) \tag{8}$$

$$M_{\mathrm{w}} = M_{\mathrm{gas}} \left(\frac{E_{\mathrm{w}}}{E_{\mathrm{bin}}}\right), \tag{9}$$

where η and ϵ are the fraction of SN explosion energy converted into the kinetic energy of the gas shells and the fraction of the kinetic energy converted into the wind energy, respectively. The definition of M_{gas} is the same as in Equation (2). The ejected mass approaches $M_{\mathrm{w}} = M_{\mathrm{gas}}$ if $\eta E_{\mathrm{SN}} \gg E_{\mathrm{bin}}$ and $M_{\mathrm{w}} = \eta\epsilon M_{\mathrm{gas}}(E_{\mathrm{SN}}/E_{\mathrm{bin}})$ if $\eta E_{\mathrm{SN}} \ll E_{\mathrm{bin}}$. We adopt fixed values of $\eta = 0.1$ and $\epsilon = 0.1$ (see Komiya et al. 2014). If M_{w} exceeds M_{sw}, we presume that all the swept-up matter is blown away, i.e., $M_{\mathrm{w}} = M_{\mathrm{sw}}$ and $M_{\mathrm{p}} = 0$.

The evolution of the mass of the metal-polluted region by the ith SN is described as follows:

$$\frac{dM_{\mathrm{p},i}}{dt} = C_{\mathrm{diff}}(t - t_i)^{1/2} - \sum_{j>i} \delta(t - t_j) M_{\mathrm{w},j} \left(\frac{M_{\mathrm{p},i}}{M_{\mathrm{gas}}}\right) - \sum_{\{k|i\in S_k\}} \delta(t - t_k) m_{*,k}. \tag{10}$$

Here t_i is the time of the ith SN explosion and $m_{*,k}$ is the mass of the kth star in the protogalaxy: the first term on the right-hand side describes the diffusion of the polluted gas. The diffusion equation in a constant density gives the time dependence of $M \propto t^{3/2}$, and hence $dM/dt \propto t^{1/2}$; the second and third terms correspond to the reduction of the polluted mass by the galactic wind driven by later SNe and by the formation of the next-generation stars, respectively; S_k is a set of the polluted regions that contribute to the formation of the

kth stars (see Section 2.2.3). If the mass of the polluted region increases to the gas mass of the protogalaxy, it stops growing and keeps the value of $M_{\mathrm{p},i} = M_{\mathrm{gas}}$ accordingly.

The diffusion coefficient, C_{diff}, which is a free parameter, is set at $10^{-6}\,M_\odot\,\mathrm{yr}^{-3/2}$ as the fiducial value. This corresponds to a reasonable environment for the formation of first stars in protogalaxies, where the gas of $\sim 2 \times 10^5\,M_\odot$ is mixed in a dynamical timescale ($\sim 3 \times 10^7$ yr) for the virialized halo at $z = 10$. Considering the turbulent mixing with the velocity v_{turb} and the scale length l_{turb}, we obtain

$$C_{\mathrm{diff}} = \frac{4\pi}{3}\left(\frac{v_{\mathrm{turb}} l_{\mathrm{turb}}}{3}\right)^{3/2} \mu n m_{\mathrm{p}} = 6 \times 10^{-7}\,M_\odot\,\mathrm{yr}^{-3/2}\left(\frac{v_{\mathrm{turb}}}{10\ \mathrm{km\ s}}\right)^{3/2}\left(\frac{l_{\mathrm{turb}}}{100\ \mathrm{pc}}\right)^{3/2} n_1 \mu, \quad (11)$$

where μ is the mean molecular weight and m_{p} the proton mass.

The mass of element species Z in the ith polluted region should have an initial value of

$$A_{Z,i} = (1 - f_{\mathrm{w},i}) Y_{Z,i}, \quad (12)$$

where $Y_{Z,i}$ is the SN yield of element Z in mass and f_{w} is the metal loading factor of the SN-driven galactic wind. The value of f_{w} is taken from the formula in Komiya et al. (2014):

$$f_{\mathrm{w}} = \min\left(1, \frac{M_{\mathrm{w}}/M_{\mathrm{sw}} + \eta E_{\mathrm{SN}}/E_{\mathrm{bin}}}{1 + \eta E_{\mathrm{SN}}/E_{\mathrm{bin}}}\right). \quad (13)$$

It approaches $M_{\mathrm{w}}/M_{\mathrm{sw}}$ if $\eta E_{\mathrm{SN}} \ll E_{\mathrm{bin}}$ and $f_{\mathrm{w}} = 1$ at the opposite limit.

The formulation of the time evolution of the mass of metals, $A_{Z,i}$, can be written in analogy to Equation (10). The mass of the metals in the ith polluted region, $A_{Z,i}$, is conserved through the diffusion. The outflow and star formation do not change the chemical composition $A_{Z,i}/M_{\mathrm{p},i}$. Therefore, the change of the mass of the metals with respect to time is given as follows:

$$\frac{dA_{Z,i}}{dt} = -\sum_j \delta(t - t_j) A_{Z,i} \frac{M_{\mathrm{w},j}}{M_{\mathrm{gas}}} - \sum_{\{k|i\in S_k\}} \delta(t - t_k) A_{Z,i} \frac{m_{*,k}}{M_{\mathrm{p},i}}. \quad (14)$$

To save a computational cost in computing inhomogeneous chemical evolution for EMP stars, we introduce a cutoff parameter for chemical enrichment. The inhomogeneous mixing by SN ejecta is switched off if the number of polluter SNe in a protogalaxy exceeds the critical value. We treat the mixing of metals in a protogalaxy as the averaged pollution if the number of SNe is more than 30, i.e.,

$$\sum_i M_{\mathrm{p},i} = 30 M_{\mathrm{gas}}, \quad (15)$$

or if the average metallicity of the protogalaxy exceeds [Fe/H] $= -1$. The fraction of gas that remains unpolluted by SNe is evaluated by $\prod_i (1 - M_{\mathrm{p},i}/M_{\mathrm{gas}})$. If all the polluted regions have the same mass of $M_{\mathrm{p}} (< M_{\mathrm{gas}})$, this value is reduced to $(1 - M_{\mathrm{p}}/M_{\mathrm{gas}})^{30 M_{\mathrm{gas}}/M_{\mathrm{p}}}$, which is below 10^{-13} for any ratios of $M_{\mathrm{p}}/M_{\mathrm{gas}}$. For any choice of M_{p}, the fraction is always small. The application of this mixing typically occurs at [Fe/H] ~ -3 in the fiducial model. We checked the validity of this model by employing a larger value for the criterion of $\sum_i M_{\mathrm{p},i} = 60 M_{\mathrm{gas}}$, which gives an almost identical result.

2.2.2. Infall of Metal-enriched Gas

We consider the gas infall onto protogalaxies in addition to the metal enrichment of IGM by the galactic wind.

As mentioned above, the first SN in a protogalaxy triggers the galactic wind into the IGM. As the protogalaxy evolves, metals and gas blown out by subsequent SNe are added to the wind. We follow the spread of the wind in the IGM assuming momentum conservation (see Komiya et al. 2014 for details).

The minihalos accrete IGM in accordance with the growth of the minihalo. Though the IGM has the pristine abundance at very early universe, the IGM around the minihalo is enriched by the wind from nearby protogalaxies and/or the wind from the minihalo itself. Therefore, the chemical abundance, $X_{\mathrm{inf},Z}$, of the infalling gas depends on time. The chemical composition of a protogalaxy can be inhomogeneous even before the first SN in the protogalaxy.

Following our previous studies, we assume that the gas infall rate is proportional to the mass evolution of the dark halo given by a merger tree. We store the data of the metallicity, $X_{\mathrm{inf},Z}(z)$, and the mass, $\Delta M_{\mathrm{gas}}(z)$, of the infall gas budget for each time step, Δz, and each branch of the merger trees. The time step is set at $\Delta z = 0.01(1 + z)$. The diffusion of metals in the ejected and infalling gas is not taken into consideration.

2.2.3. Stellar Abundances

The chemical abundance of stars is given by the sum of the elements for metals, Z, carried by the infalling gas, and taken from the metal-polluted regions by SNe. When a kth star is formed, we randomly select an infall gas budget with the probability proportional to the mass, $\Delta M_{\mathrm{gas}}(z)$, of each gas budget. Then, we randomly determine whether the star is in the ith polluted region or not (i.e., $i \in S_k$ or not) by the probability of $M_{\mathrm{p},i}/M_{\mathrm{gas}}$, for each of all the polluted regions by SNe. We compute the sum of the chemical abundance of the selected infall gas budget and the polluted region, in which the star is formed,

$$X_{k,Z} = X_{\mathrm{inf},Z} + \sum_{\{k|i\in S_k\}} \frac{A_{Z,i}}{M_{\mathrm{p},i}}, \quad (16)$$

and record this value as the abundance of the kth star.

2.3. Faint Supernovae

The yields of faint SNe are determined by a free parameter to produce a wide range of the observed values of [C/Fe] in CEMP-no stars. We introduced a fallback parameter f_{fb} to control the value of [C/Fe] by decreasing the iron yield by a factor of f_{fb}, keeping the carbon yield unchanged. We adopted chemical yields by Kobayashi et al. (2006), where the systematic mass dependence of the yields from normal SNe is available. The choice of the parameter from 0.1 to 10^{-5} produces the observed range of $1 \lesssim$ [C/Fe] $\lesssim 5$ for CEMP-no stars. The values of f_{fb} are subject to the log-flat distribution in the range of 0.1–10^{-5}. Comparisons are made only for carbon and iron abundances in this study.

The occurrence of faint SNe is also determined by a free parameter owing to our poor knowledge on the formation of SNe, i.e., we do not know the ratio of faint SNe to normal SNe,

Table 1
Key Parameters and Values in the *StarTree* Code

Parameter	Description	Fiducial Value	Other Tested Values
$\epsilon_\star$	Star formation efficiency	$1.2 \times 10^{-14}\,\mathrm{yr}^{-1}$	$5 \times 10^{-11}\,\mathrm{yr}^{-1}$
$\dot{M}_*$	Star formation rate	$\epsilon_\star M_{\rm gas}$	n/a
f_b	Binary fraction	50%	n/a
$M_{\rm md}$	Peak mass of the IMF	$10\,M_\odot$ for Population III and $3\,M_\odot$ for EMP stars	$100\,M_\odot$ for Population III
$M_{{\rm sw},i}$	Swept-up mass by the ith SN	$5.1 \times 10^4\,M_\odot$	$5.1 \times 10^{-3}\,M_\odot$
$M_{{\rm w},i}$	Mass of the galactic wind triggered by the ith SN	n/a[a]	n/a
$M_{{\rm p},i}$	Mass of the polluted region occupied by the ith SN	Equations (5) and (10)	n/a
$E_{\rm SN}$	Explosion energy of the SN	10^{51} erg	n/a
$E_{\rm bin}$	Binding energy of the protogalaxy	n/a[a]	n/a
$C_{\rm diff}$	Diffusion coefficient for ISM mixing by SN ejecta	$10^{-6}M_\odot\,\mathrm{yr}^{-3/2}$	$10^{-5}M_\odot\,\mathrm{yr}^{-3/2}$, $10^{-7}M_\odot\,\mathrm{yr}^{-3/2}$
$f_{\rm w}$	Metal loading factor of the SN-driven galactic wind	Equation (13)	n/a
$f_{\rm fb}$	Fallback parameter of faint SNe	log-flat distribution in 0.1–10^{-5}	n/a
$Z_{\rm cr}$	Critical metallicity for faint SNe	$10^{-5}Z_\odot$	$10^{-3}Z_\odot$

Note.
[a] The values are computed internally. See text for details.

and how it depends on mass and metallicity. We tested the case with the most efficient contribution of faint SNe by introducing the critical metallicity, $Z_{\rm cr}$, below which all the massive stars end their lives as faint SNe. The fiducial value of $Z_{\rm cr} = 10^{-5}\,Z_\odot$ is adopted. The results with the other choice of this parameter are discussed in Section 3.2.2.

The key parameters in the *StarTree* code are provided in Table 1. The second, third, and fourth columns represent the meaning of the parameter, the fiducial value, and other values to examine parameter dependence, respectively.

3. Results and Discussion

3.1. Fiducial Model

Our fiducial model produced ∼160,000 faint SNe, where we found two to three faint SNe per branch of the merger tree. Most of their progenitors are Population III stars, with the minor contribution of ∼15,000 second-generation stars having $Z \leqslant Z_{\rm cr}$.

Figure 4 shows the explosion epoch and the mass of their host minihalos for faint SNe (red), low-mass CEMP stars (blue), and EMP stars (gray). In a minihalo of mass with $M_{\rm h} \lesssim 10^6\,M_\odot$, faint or normal SNe blow off most of the gas from the host halo. Even in this case, there is still a channel of CEMP star formation if the minihalo attains the blown-off gas by fallback. A majority of faint SNe take place in minihalos with a mass $M_{\rm h} < 10^7\,M_\odot$, while only 15% of CEMP stars are formed in minihalos in this mass range. Approximately 70% of CEMP stars are formed in halos with a mass of 10^7–$10^8\,M_\odot$.

Figures 5 and 6 show the distribution of the iron and carbon abundances and the metallicity distribution function (MDF) for the low-mass stars that survive to date, respectively. In Figure 5, the HMP and lower-metallicity stars ([Fe/H] $\leqslant -5$) in the model show carbon enhancement ([C/Fe] $\geqslant 0.7$), and yet the carbon abundance is confined below [C/H] $\lesssim -2.5$, significantly lower than observed from CRUMP stars. For UMP stars of $-5 <$ [Fe/H] $\leqslant -4$, a majority of stars are predicted below [C/Fe] $= 0.7$ and scarcely show carbon enhancement. For higher metallicity, only a small fraction of stars show carbon enhancement, while their carbon abundances increase with iron abundances. The majority of stars with the largest carbon abundances are originated from the fallback gas, i.e., ejected

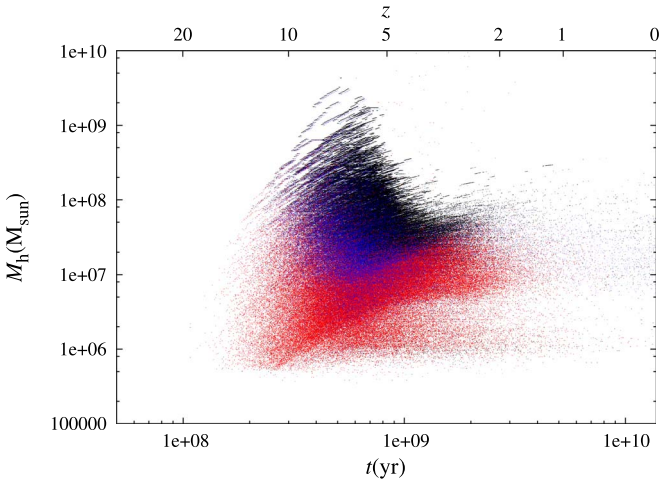

Figure 4. Time from the big bang (abscissa) and the mass of the host minihalos (ordinate) of faint SNe (red). Also plotted are the formation time (or redshift on the top) and the host halo mass of CEMP stars (blue) and EMP stars (gray) for [Fe/H] < -3, which mostly overlap with the data points of faint SNe except for the later stages of evolution with larger mass of host halos.

from host halo by the SN-driven galactic wind, and then reaccreted onto themselves.

There are no stars distributed in the large carbon abundance above [C/H] > -2.5 in this model for [Fe/H] $\lesssim -3$. This is because the carbon abundance of a polluted region just after a faint-SN explosion is determined by

$$[{\rm C/H}] \simeq \log\left(\frac{\Delta M_{\rm C}/X_{\rm C\odot}}{M_{\rm sw}X_{\rm H,gas}/X_{\rm H\odot}}\right) \sim -2.5, \qquad (17)$$

from the carbon budget ($\Delta M_{\rm C} = 0.2\,M_\odot$) and the swept-up mass ($M_{\rm sw} = M_{\rm ws51}$) of faint SNe. This sets an upper limit on [C/H] of the second-generation stars. The location of [Fe/H] of the second-generation stars on the line of constant [C/H] depends on the fallback parameter $f_{\rm fb}$ in faint SNe, which controls the carbon enhancement, [C/Fe].

In the polluted region by the accretion of IGM gas, the carbon and iron abundances are further reduced by mixing with

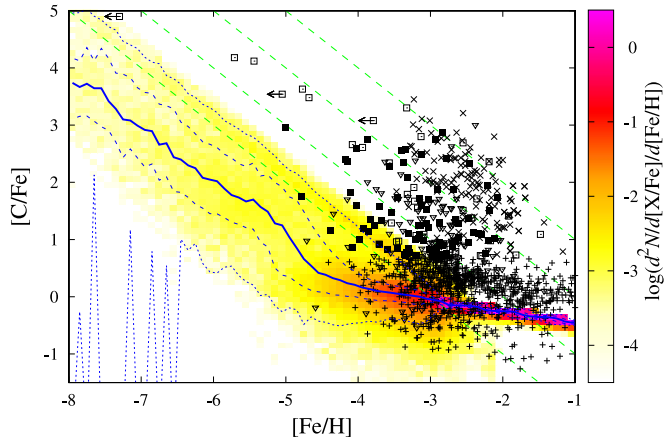

Figure 5. Distribution of the metal-poor stars on the metallicity ([Fe/H]) and the carbon enhancement ([C/Fe]) diagram. The predicted distribution is color-coded as illustrated in the right margin. Blue lines show the percentile curves of 5%, 25%, 50%, 75%, and 95% in each metallicity bin for the predicted distribution. Black symbols denote the observed data of stars, taken from the SAGA database, which have the same meanings as in Figure 1. Diagonal dashed (green) lines indicate the loci of constant carbon abundances of $[C/H] = 0, -1, -2, -3$ from top to bottom, respectively.

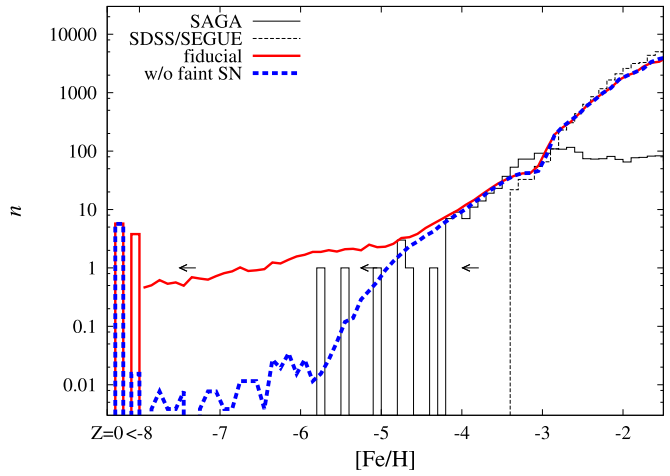

Figure 6. MDFs of low-mass stars that survive to date. Red and blue lines show the model results with and without faint SNe; two pillars on the left end denote the numbers of stars with $Z = 0$ and with a finite metallicity of $[Fe/H] < -8$, respectively. Solid and dashed histograms denote the observed MDFs for the SAGA database sample and for the SDSS/SEGUE data (Carollo et al. 2010), respectively. The former sample stars have the accurate metallicity with the high-resolution spectroscopy but are biased toward lower metallicity ($[Fe/H] \lesssim -2.5$), while the latter is a homogeneous sample but has the metallicity only by medium-resolution spectroscopy ($[Fe/H] \gtrsim -3$). Horizontal arrows denote the upper limit of [Fe/H] for stars without the detection of iron.

the ISM through the diffusion, where stars with lower [C/H] are formed. Since both iron and carbon are diluted in the same way, the abundance ratios of carbon to iron will not change by the diffusion. In such a case, the stars move horizontally to the left on the [Fe/H] and [C/Fe] plane. CEMP stars are formed in the protogalaxies with typical gas mass of $M_{gas} \simeq 10^6$–$10^7\ M_\odot$ and are distributed around $[C/H] \simeq -4$.

A minor population of second-generation stars having $Z < Z_{cr}$ are formed out of the first SN ejecta mixed with the ISM of mass larger than $\sim 10^7\ M_\odot$. They compose only $\sim 2\%$ of the total number of faint SNe in the fiducial model. On the other hand, a majority of stars with $[Fe/H] > -5$ are formed around $[C/H] \simeq 0$. These carbon-normal stars are the third or later generations of stars and are formed of gas polluted by a single or multiple normal SNe.

The fiducial model fails to explain the stars with a large value of [C/H] among observed CRUMP stars, even if we consider the uncertainties of our models associated with the assumptions. For instance, it is possible to reproduce large carbon abundances by considering chemical inhomogeneity in minihalos, caused by the pollution of a single faint SN. However, the swept-up mass and the diffusion coefficient of SN yields have to be smaller by more than an order of magnitude than our fiducial value because typical carbon abundances of the second-generation stars are significantly lower than the observed CRUMP stars. This is discussed in Section 3.2.5.

Figure 5 also indicates that only a few CEMP stars are formed from the gas with $[Fe/H] \gtrsim -3$. In particular, it is unlikely that faint SNe contributed to the formation of the Group I CEMP stars with $[C/H] \gtrsim -1$, which demands the condensation of carbon in the ISM by more than 100 times than what is realized in our models. Although the majority of the Group I stars are made up of CEMP-*s* stars, which are generally thought to be formed by a binary mass transfer from low-mass AGB stars, there are more than 10 CEMP-no stars with $[C/H] > -1$. A formation mechanism(s) other than a faint SN is (are) required for these CEMP-no stars with very high carbon abundances. We have argued in a separate paper that they are formed by a binary mass transfer in the same way as CEMP-*s* stars with differences in progenitor mass and the efficiency of the *s*-process nucleosynthesis in primary stars, where high-mass AGB stars and low efficiencies in the *s*-process nucleosynthesis as primary stars are required (Komiya et al. 2007; see also S. Yamada et al. 2020b, in preparation).

In Figure 6, we compare the MDF of the low-mass survivors for the fiducial models with and without the faint SNe. Both model MDFs coincide with each other in the metallicity range of $[Fe/H] \gtrsim -4$ and also predict a similar number of Population III stars. The difference between these two model MDFs lies only in the number of HMP and lower-metallicity stars below $Z \lesssim Z_{cr}$, i.e., with $[Fe/H] \lesssim -5$. The model with faint SNe produces an almost flat MDF at lower metallicity, while the model without the faint SNe produces an MDF that significantly decreases the number of HMP stars. This is expected from the fact that smaller metallicity demands greater dilution of SN yields by the diffusion in the polluted regions. The difference in the number of HMP stars between the two models grows larger to be two orders of magnitude for the low metallicity of $[Fe/H] < -6$. In the model without faint SNe, such low-metallicity stars are formed in the minihalos, already polluted by the galactic wind, prior to the star formation (see below). In both MDFs, we see a small dent near $[Fe/H] \simeq -3$, which is an artifact of averaging the chemical composition by the criterion of Equation (15). Otherwise, the slope will be almost constant and a linearity relationship nearly holds between the metallicity and the number of low-mass survivors for $[Fe/H] \gtrsim -4$.

The observed MDFs in Figure 6 represent the data taken from the SAGA database and the Sloan Digital Sky Survey (SDSS)/SEGUE sample (Carollo et al. 2010) to compare with the model predictions. The SAGA database collects literature data of those stars that have the abundances derived from high- and medium-resolution spectra, which provides the largest sample of EMP stars. It is to be noted that the determination of

the metallicity of [Fe/H] $\lesssim -3$ requires high-resolution follow-up observations. Since the high-resolution observations are biased toward the low metallicity of [Fe/H] $\lesssim -2.5$, the sample stars are not complete at larger metallicities. On the other hand, the SDSS/SEGUE sample provides relatively unbiased and homogeneous data. However, the metallicities of their sample stars are not reliable for [Fe/H] $\lesssim -3$ since they are determined by the medium-resolution spectroscopic data, and the sample size is small for [Fe/H] < -3. It is argued that the SAGA database sample is almost unbiased below [Fe/H] $\leqslant -2.8$ (Suda et al. 2008). Thus, we may scale the MDF from the SDSS/SEGUE sample to match the MDF from the SAGA database at the bin between [Fe/H] $= -2.8$ and -2.9. We combined two MDFs at [Fe/H] $= -2.8$ below and above which the SAGA database and the SDSS/SEGUE sample are adopted, respectively. We scale them to match the model MDFs.

Both model MDFs with and without faint SNe are consistent with the observations at [Fe/H] $\gtrsim -4$. At $-5 <$ [Fe/H] < -4.2, both models tend to predict slightly more stars than observed. For [Fe/H] < -5, the model with faint SNe gives a much larger number of stars than observed by more than 1 dex. In contrast, the model without faint SNe achieves much better consistency with the observed MDF, though the observational sample of HMP stars is small, The most iron-poor star ever detected is SMSS J031300.36–670839.3 with [Fe/H] < -7.3 (Keller et al. 2014; Bessell et al. 2015). In the model without faint SNe, the number of predicted stars below [Fe/H] $= -7$ is very small, but it is expected to find approximately one star between $-\infty <$ [Fe/H] < -7.

We note that approximately six Population III stars are predicted regardless of the models with or without faint SNe. The absence of strict Population III stars in the current sample is indicative that the frequency of low-mass stars among Population III stars is significantly lower than among HMP stars. Although the shape of the IMF of Population III stars is not well understood, higher-mass IMFs are favored by theoretical studies. As discussed in our previous studies and in later sections of this paper, the accretion of the interstellar gas polluted by SN yields after the birth can significantly change the MDF for [Fe/H] $\lesssim -4$ and can explain the absence of Population III stars and the lowest-metallicity tail of the MDF.

3.1.1. External Enrichment of Minihalos

The external enrichment has been discussed as a formation scenario for the most low-metallicity Population II stars (Smith et al. 2015; Chiaki et al. 2018a). Energetic Population III SNe in minihalos can blow away the metals from their host minihalos and enrich the IGM around the host minihalos, as well as the nearby minihalos with the metals. The nearby minihalos or the minihalos that accrete the metal-enriched IGM can form the second-generation stars with very low metallicity.

We found that the external enrichment plays a minor role in the fiducial model. Only 1% of HMP stars are the first-generation stars in the minihalos enriched by the external pollution. In our model, most of the ejected metals fall back to its progenitor protogalaxy as the protogalaxy increases its mass.

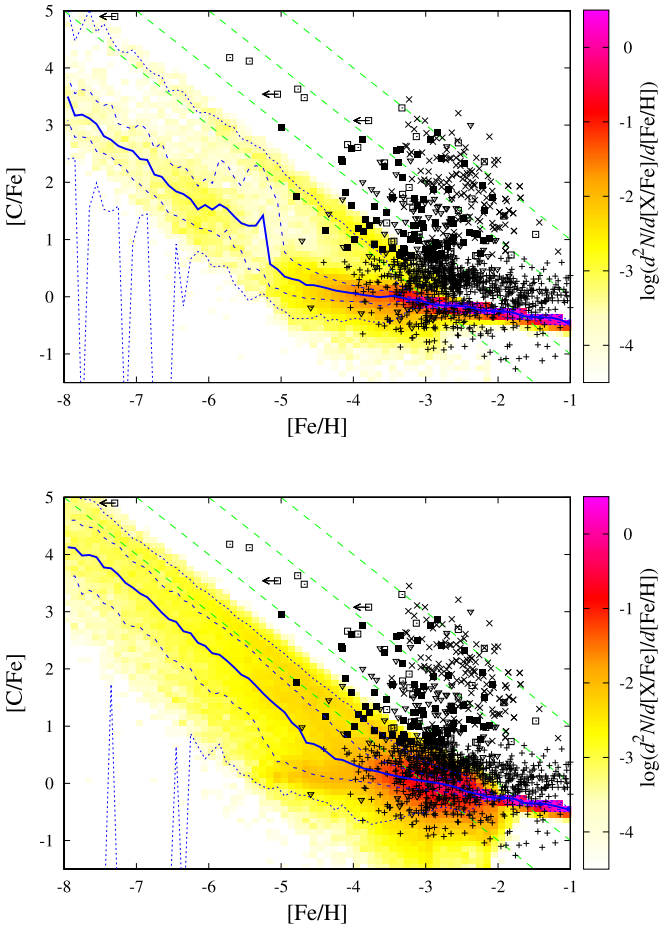

Figure 7. Same as Figure 5, but for the model of the diffusion coefficient, $C_{\rm diff} = 10^{-5}\,M_\odot\ {\rm yr}^{-3/2}$ (top panel), and the model of $C_{\rm diff} = 10^{-7}\,M_\odot\ {\rm yr}^{-3/2}$ (bottom panel).

3.2. Parameter Dependences

Our fiducial model fails to reproduce the distribution of stars on the [C/H]–[Fe/H] plane. Here we try to find the parameter set that can reproduce the observations in the framework of the faint-SN scenario.

3.2.1. Mixing Mass of SN Ejecta

Initial carbon abundance, [C/H], of the polluted region is in inverse proportion to the mixing mass as described in Equation (17). In models with smaller values of diffusion coefficient, $C_{\rm diff}$, and swept-up mass, $M_{\rm sw51}$, the second-generation stars will have higher [C/H]. In this case, a larger number of Population III stars are formed and explode as faint SNe since the progress of metal pollution in the ISM is slower than what is realized with larger values of $C_{\rm diff}$ and/or $M_{\rm sw51}$.

Figure 7 shows the dependence on the diffusion coefficient, $C_{\rm diff}$. In the slow diffusion model with $C_{\rm diff} = 10^{-7}\,M_\odot\ {\rm yr}^{-3/2}$ (bottom panel), the metals ejected by an SN are mixed and diffuse only over the mass of $\sim 10^5\,M_\odot$ after 10^8 yr. This model predicts higher [C/H] for UMP/HMP stars than the fiducial model as a whole, and yet most of them are still distributed below [C/H] $\lesssim -3$.

In the fast diffusion model with $C_{\rm diff} = 10^{-5}\,M_\odot\ {\rm yr}^{-3/2}$ (top panel), on the other hand, we see two branches for [Fe/H] < -4. One is at slightly above [C/H] ~ -3, and the other is around [C/H] ~ -4.5. The former branch corresponds

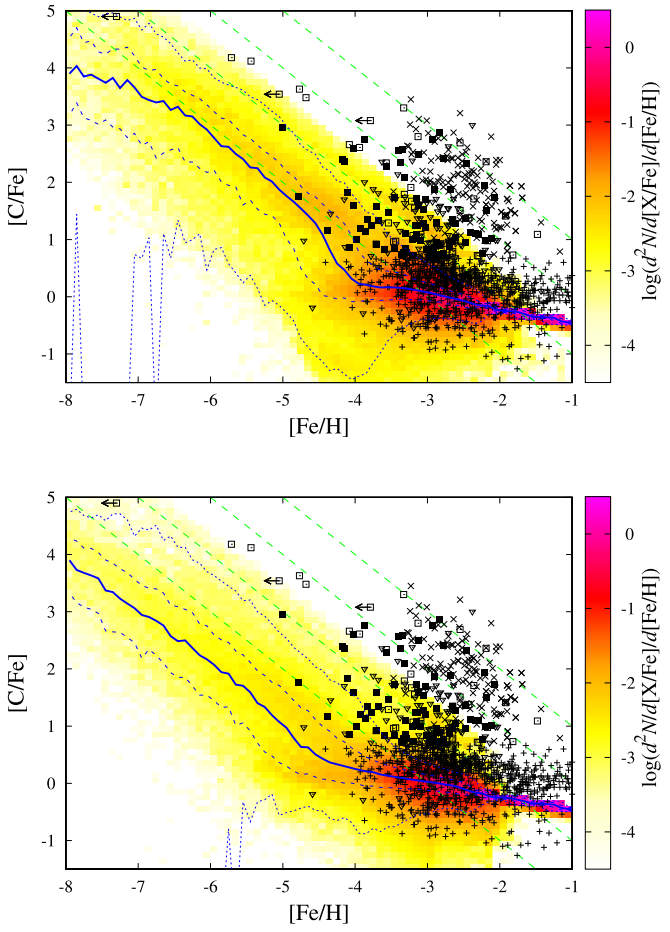

Figure 8. Dependence on the swept-up mass, $M_{\rm sw51}$. In the top panel we adopt a factor of 10 smaller mass, $M_{\rm sw51} = 5.1 \times 10^3\,M_\odot$. In the bottom panel, we assume the fiducial value of $M_{\rm sw51}$ but the explosion energy to be smaller by a factor of 10, i.e., $E_{\rm SN} = 10^{50}$ erg, for faint SNe. In both models, the small diffusion coefficient, $C_{\rm diff} = 10^{-7}\,M_\odot\ {\rm yr}^{-3/2}$, is adopted.

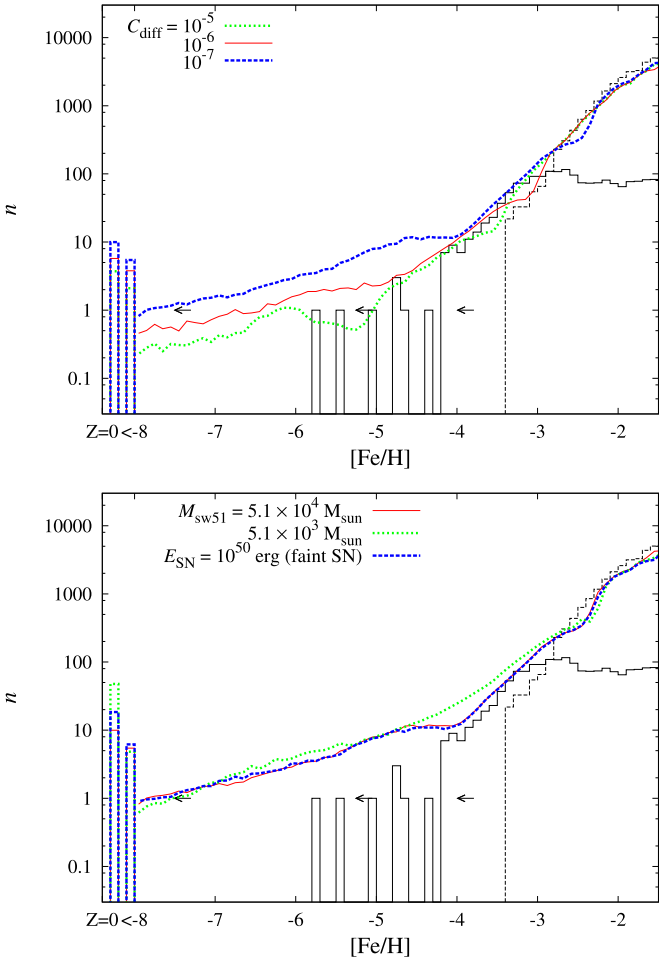

Figure 9. Dependence of MDF on the $C_{\rm diff}$ (top panel) and $M_{\rm sw}$ (bottom panel).

to the upper limit of [C/H] given in Equation (17). The majority of these stars are formed in the reaccreted gas, enriched by the outflow from its own protogalaxy. An SN triggers the galactic wind from minihalos and enriches the surrounding IGM, where the chemical composition of the wind is [C/H] ~ -2.5. Reaccreted gas onto the protogalaxy contains metals contaminated by the outflow, driven by SNe from the former host galaxy. Since the metal diffusion is neglected for the reaccreted gas in the present computations, the stars formed of the reaccreted gas have carbon abundances similar to those of galactic wind. If we take into account the diffusion of reaccreted metals, the number of stars in the high-[C/H] branch will be smaller. In the model with the small $C_{\rm diff}$, the lower branch is shifted toward higher [C/H] and overlaps with the upper branch.

The stars in the lower branch are formed in the protogalaxy with a gas mass of $M_{\rm gas} = 10^6$–$10^7\,M_\odot$. The mixed ejecta of one or a few faint SN(e) form stars in this branch.

In models with $M_{\rm sw51} = 5.1 \times 10^3\,M_\odot$, stars with [C/H] > -2 can be formed, as shown in Figure 8. Since the upper limit of carbon abundances in Equation (17) increases to [C/H] $\simeq -1.5$, they have the comparable carbon abundance with the observed CRUMP stars. However, the number of stars with [C/H] > -2 is still very small, and the vast majority of UMP/HMP stars have [C/H] < -3.

The impact of reducing the explosion energy is similar to that of the lower $M_{\rm sw51}$ case as shown by the bottom panel of Figure 8. The combined effects of low-energy SNe and less efficient mixing of ejecta with the ISM do not provide a sufficient number of CRUMP stars with [C/H] > -2. According to the models of Tominaga et al. (2013), most of the known CRUMP stars can be reproduced by the models with $E_{\rm SN} = 10^{51}$ erg. These suggest that low-energy SNe are not necessarily responsible for the contribution to the CRUMP stars.

Figure 9 shows the dependence of MDFs on $C_{\rm diff}$ (top panel) and the swept-up mass (bottom panel). The distribution at [Fe/H] > -4 is independent of $C_{\rm diff}$ except for the dip due to the artificial averaging of chemical composition by the criterion of Equation (15), which occurs at [Fe/H] ~ -2.5, -3, and -3.5 for models of $C_{\rm diff} = 10^{-7}$, 10^{-6}, and $10^{-5}\,M_\odot\ {\rm yr}^{-3/2}$, respectively. On the other hand, the number of UMP/HMP stars and Population III stars is sensitive to $C_{\rm diff}$. In the case of smaller $C_{\rm diff}$, the metal enrichment process of protogalaxies is delayed, which produces more faint SNe. As a result, more second-generation UMP/HMP stars are formed. For $C_{\rm diff} = 10^{-8}\,M_\odot\ {\rm yr}^{-3/2}$, the result is quite similar to that for $C_{\rm diff} = 10^{-7}\,M_\odot\ {\rm yr}^{-3/2}$.

The smaller the value of $M_{\rm sw}$ (with $M_{\rm w}$ unchanged), the larger the number of Population III stars since the ISM gas in the protogalaxy remains with $Z = 0$. Smaller polluted masses around many faint SNe tend to produce metal-rich second-generation stars

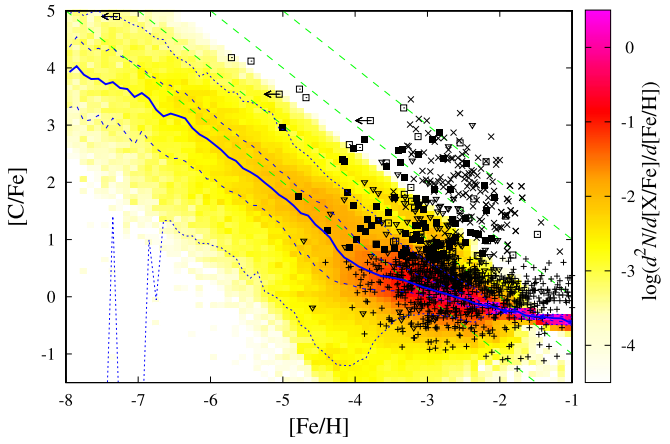

Figure 10. Model with $Z_{\rm cr} = 10^{-3}\,Z_{\odot}$. Other parameters are the same as in the case of the top panel of Figure 8 ($M_{\rm sw51} = 5.1 \times 10^3\,M_{\odot}$ and $C_{\rm diff} = 10^{-7}\,M_{\odot}\,{\rm yr}^{-3/2}$).

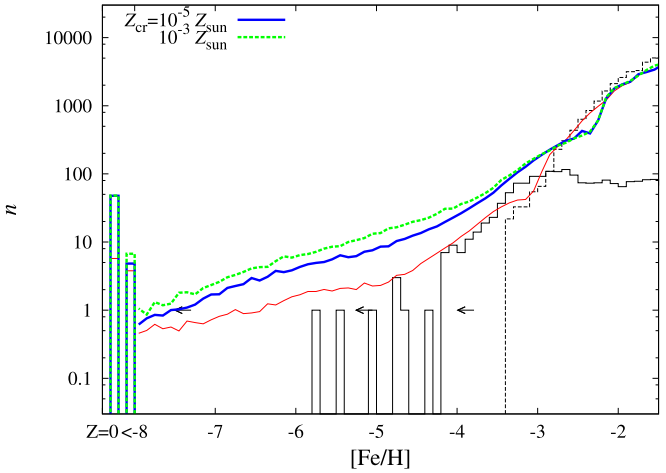

Figure 11. MDFs of the model with $Z_{\rm cr} = 10^{-3}$ (green) and $Z_{\rm cr} = 10^{-5}$ (blue), for which small mixing parameters are assumed ($C_{\rm diff} = 10^{-7}\,M_{\odot}\,{\rm yr}^{-3/2}$ and $M_{\rm sw} = 5.1 \times 10^3\,M_{\odot}$). We also plot the result of the fiducial model (red).

owing to the enrichment of ISM by other faint SNe. In addition, most of the SN ejecta participate in outflows because the ratio, $M_{\rm w}/M_{\rm sw}$, becomes larger (see Equation (9)). The ejecta accrete onto their host minihalos as they grow in mass, where we do not consider the metal diffusion, which preserves the region of $Z = 0$ and increases the chance for faint SNe in the host halo. Both of these effects contribute to the increase in the number of stars around [Fe/H] ~ -4. We found ∼1,600,000 faint SNe in this case, which is ∼10 times more than the case in the fiducial model.

3.2.2. Criterion for Faint SN

In the fiducial model, all the SNe are assumed to be faint SNe if the metallicity is below the critical metallicity, $Z_{\rm cr} = 10^{-5}\,Z_{\odot}$. Figures 10 and 11 show the results with $Z_{\rm cr} = 10^{-3}\,Z_{\odot}$. We adopt the smaller diffusion rate of $C_{\rm diff} = 10^{-7}\,M_{\odot}\,{\rm yr}^{-3/2}$ and the smaller swept-up mass of $M_{\rm sw51} = 5.1 \times 10^3\,M_{\odot}$ compared with the fiducial model in order to obtain more stars with larger [C/H]. As a result, more than a quarter of stars evolve to CEMP stars for [Fe/H] < -3.8, and the majority of them have [C/Fe] > 0.7 by the chemical enrichment up to [Fe/H] $\simeq -4.2$. This result shows the possibility that the Group II stars with weak carbon enhancement are originated from faint SNe. However, as in the fiducial model, the predicted carbon abundances of CEMP stars are much lower than CEMP stars in Group I or Group III. We need an additional source of carbon in this framework.

The metallicity of the second-generation stars is controlled by the fallback parameter $f_{\rm fb}$ (defined in Section 3.1) for which all the Population III stars end their lives as faint SNe with log-flat distribution in the metallicity range of [Fe/H] $= -5$ to -1. Changing the distribution of $f_{\rm fb}$ does not solve the discrepancy of the [C/H] values between the model and observed stars because $f_{\rm fb}$ only changes iron abundances, keeping carbon abundances unchanged. Furthermore, we should note that the assumption on $f_{\rm fb}$ provides an optimistic case for the number of CEMP stars because the number of carbon-normal stars will increase by considering the case that Population III stars end their lives as normal SNe.

Theoretically, the distribution of $f_{\rm fb}$ is a determinant of the number ratio of HMP/UMP stars, provided that most of them are descendants of first-generation stars ending their lives by faint SNe. The larger the value of $f_{\rm fb}$, the smaller the metallicity

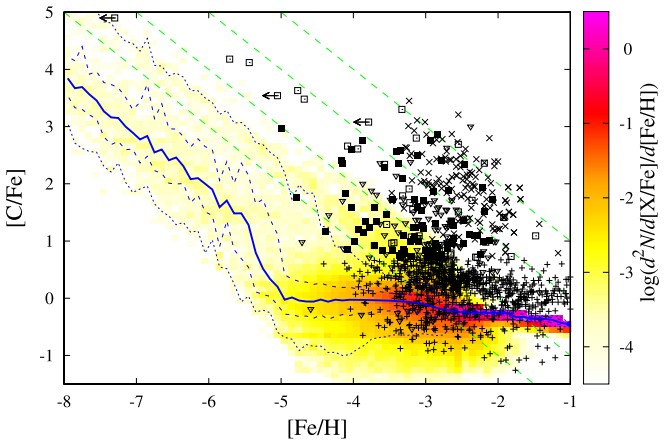

Figure 12. Same as Figure 5, but for the model with the IMF of the peak mass $M_{\rm md} = 100\,M_{\odot}$ for Population III stars.

of a second-generation star, hence increasing the number of HMP stars relative to UMP stars. Observationally, the number of CEMP stars with [C/Fe] ~ 1 is more abundant than CEMP stars with very high [C/Fe] of 3–4 (Suda et al. 2011; Norris et al. 2013). This indicates that a higher value for $f_{\rm fb}$ is preferred.

3.2.3. Population III IMF

Changing the IMF has an impact on the values of [C/Fe] through the contribution from progenitors with different initial masses. Since the carbon yield is not sensitive to the progenitor mass, carbon abundances in HMP/UMP stars are almost independent of the IMF in considering core-collapse SNe. In contrast, pair-instability SNe (PISNe) can be important if we consider the IMF including very massive stars. Figures 12 and 13 show the carbon enhancement and the MDF for the model with the IMF of $M_{\rm md} = 100\,M_{\odot}$ for Population III stars. We assume that massive stars with 50–140 $M_{\odot}$ fail to explode and collapse to black holes, and that stars with 140–270 $M_{\odot}$ explode as PISNe. In this model, ∼14,000 PISNe take place. The number of CEMP stars and lower-metallicity stars including HMP/UMP stars is relatively smaller than that in the fiducial model. This is partly because the frequency of faint SNe decreases. Another factor is the competition between the

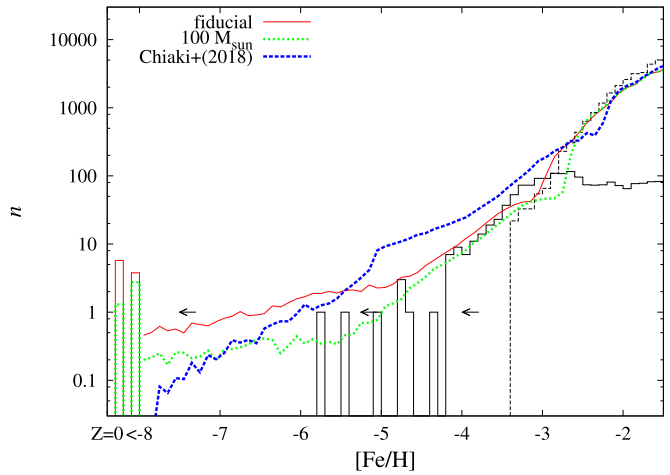

Figure 13. MDFs of the model with $M_{\rm md,Pop3} = 100\,M_\odot$, where $C_{\rm diff} = 10^{-7}\,M_\odot\,{\rm yr}^{-3/2}$, $M_{\rm sw51} = 5.1 \times 10^3\,M_\odot$, and $Z_{\rm cr} = 10^{-4}\,Z_\odot$ are adopted (green line). The model with the low-mass star formation criterion of Chiaki et al. (2018b; blue line) is compared with the fiducial model (red line).

large production of iron from a single PISN and the pollution of a large area with metals by the ejecta of a PISN.

It is argued that a PISN of $\sim$150 $M_\odot$ ejects a larger amount of carbon but a smaller amount of iron compared with CCSNe (Umeda & Nomoto 2002). These PISNe will contribute to the stars with the highest carbon abundance of [C/H] ~ -2. However, this is not supported by the abundance patterns of other elements in CEMP stars. The PISN yields show a large enhancement of elements with even atomic numbers from carbon through calcium, as well as a deficiency of odd-Z elements, which is not the case for CEMP stars.

Changing the IMF for EMP stars does not have a significant effect. The change of the mean peak mass for EMP stars is not subject to a great uncertainty because the SN yields are not so sensitive to the initial mass, as stated above. For instance, the mean peak mass of 10 $M_\odot$ does not change the result very much. On the other hand, the peak mass of 40 $M_\odot$ may enhance the fraction of C-rich stars. However, this is not a favored assumption from the constraints on the number of known EMP stars at present, which is discussed in Komiya et al. (2009b).

3.2.4. Star Formation Efficiency

A constant SFE is examined in this subsection. We adopt mass-dependent SFE in the fiducial model, i.e., the star formation rate per unit gas mass is equal to $\epsilon_\star \propto M_{\rm h}^{0.3}$ following Komiya et al. (2016). Lower values of SFE are favored in low-mass galaxies to reproduce the mass–metallicity relation of dwarf galaxies and to explain the origin of r-process elements in EMP stars through nucleosynthesis in merging neutron stars (Komiya et al. 2016). On the other hand, the SFE in protogalaxies at high redshift is not yet well understood and is parameterized in this study.

We show the model results with a constant SFE in Figures 14 and 15. The value of SFE is chosen to yield the solar metallicity at $z = 0$ for both the constant and the mass-dependent SFE, which gives $\epsilon_\star = 5 \times 10^{-11}\,{\rm yr}^{-1}$ and $1.2 \times 10^{-14}(M_{\rm h}/M_\odot)^{0.3}$, respectively. The star formation rate for constant SFE is higher than that for the mass-dependent SFE by $\sim$2 dex in minihalos of mass $M_{\rm h} = 10^6\,M_\odot$. The higher star formation rate produces more stars before the metal

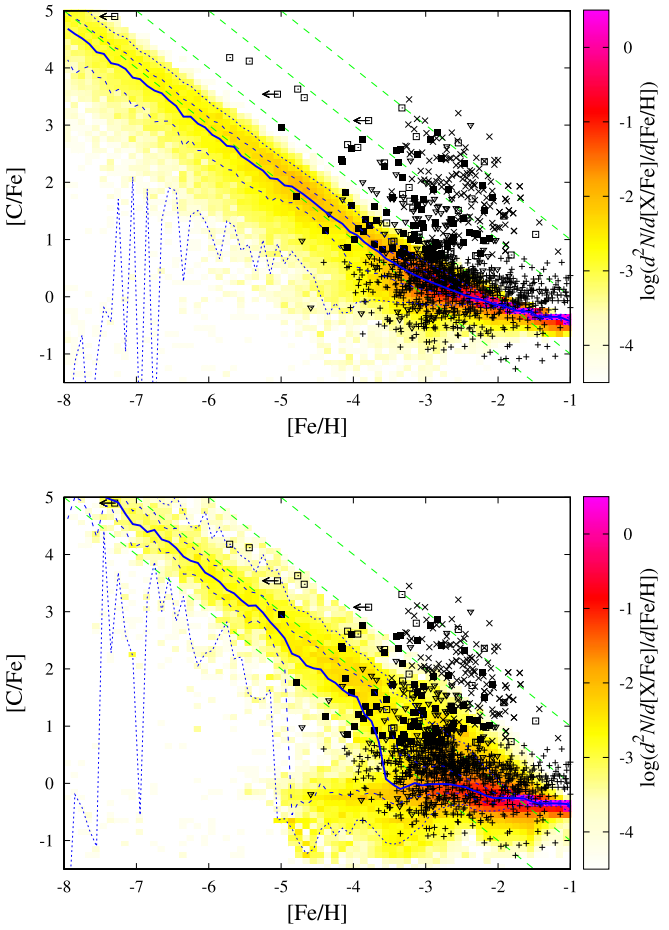

Figure 14. Models with a constant SFE ($\epsilon_\star = 5 \times 10^{11}\,{\rm yr}^{-1}$). Other parameters are fixed to the fiducial values (top panel), and the model with $M_{\rm sw51} = 5 \times 10^3\,M_\odot$, $Z_{\rm cr} = 10^{-4}\,Z_\odot$, and $M_{\rm md} = 50\,M_\odot$ for the Population III stars (bottom panel).

diffusion becomes efficient in low-mass minihalos. The change of SFE helps to increase carbon abundances by increasing the number of faint SNe, but it is still difficult to form stars with high [C/H] with these models. The distribution of HMP/UMP stars is concentrated around [C/H] ~ -3 by employing the fiducial values for other parameters.

Also, more SNe in the low-mass minihalos result in more efficient gas outflow. This reduces the gas mass in protogalaxies and hence the number of EMP stars with [Fe/H] ~ -3. The number of such EMP stars is 0.6 times smaller in the constant SFE model than in the fiducial model. Therefore, the number of HMP/UMP stars is apparently large in the case of constant SFE because the MDFs are scaled to match the observations at [Fe/H] ~ -3 in Figure 15.

3.2.5. Optimum Models

From the parameter dependences discussed above, we may choose the best-fit parameters to reproduce the observed distribution of carbon abundances of CEMP stars. In the bottom panel of Figure 14, we present the result of the model with the constant SFE, the small swept-up mass ($M_{\rm sw51} = 5.1 \times 10^3\,M_\odot$), the large critical metallicity for faint SNe ($Z_{\rm cr} = 10^{-4}\,Z_\odot$), and the massive IMF ($M_{\rm md} = 50\,M_\odot$). The predicted distribution of CEMP stars almost covers the observations

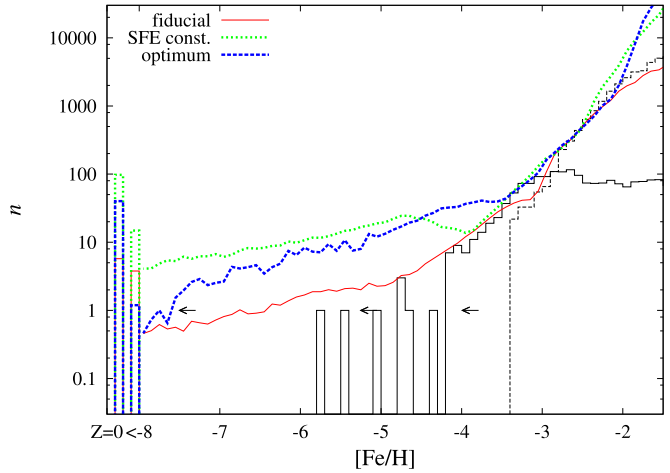

Figure 15. MDFs of constant SFE models. The green and blue lines represent the models in the top and bottom panels of Figure 14, respectively.

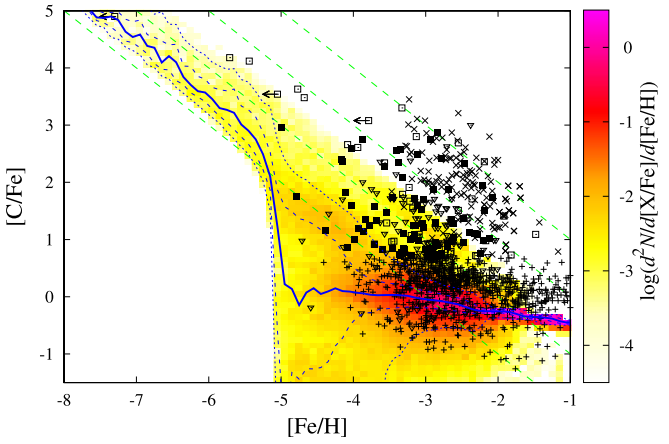

Figure 16. Model with low-mass star formation only for $10^{[C/H]-2.30} + 10^{[Fe/H]} > 10^{-5.07}$ (Chiaki et al. 2018b). Other parameters are chosen to favorably form CRUMP stars (see text).

except for the Group I CEMP stars with $[C/H] \gtrsim -1$. The difficulty of the model is the overproduction of HMP/UMP stars due to the small diffusion rate. The fraction of HMP/UMP stars can be decreased by large diffusion coefficients, but it reduces the overall carbon abundances. In this model, most of the HMP stars show large carbon enhancement with $[C/H] > -3$. In particular, the most carbon-enhanced stars are produced by PISNe, as mentioned in Section 3.2.3. However, this result is likely to be a numerical artifact. The main reason for the large carbon enhancement in PISNe is that we ignored the mixing of ejecta by the diffusion process for infall gas, as described in Section 3.2.1. Accordingly, the gas with large [C/H] is localized in minihalos that experienced PISNe.

Another way to produce carbon enhancement in HMP stars is to allow the formation of low-mass stars by setting a critical carbon abundance. This is the case in Chiaki et al. (2018b), who gave the critical carbon and iron abundances, based on the observed abundance distribution of EMP stars and on the gas cooling by carbon grains and silicate grains. They proposed that low-mass stars are formed only when

$$10^{[C/H]-2.30} + 10^{[Fe/H]} > 10^{-5.07}. \quad (18)$$

We adopt this criterion on the model with the other parameters set favorable to form CRUMP stars: $Z_{cr} = 10^{-4}\,Z_\odot$, $C_{diff} = 10^{-7}\,M_\odot\,yr^{-3/2}$, and $E_{SN} = 10^{50}$ erg for faint SNe. The result is shown in Figure 16.

In this model, HMP stars are distributed above $[C/H] > -3$ as a natural consequence of the criterion, but the distribution of stars with the carbon and iron abundances above the criterion is almost identical to the model assuming the low-mass IMF for Population III stars. We see a discrepancy between the model result and the observations. At $-5.07 < [Fe/H] < -4$, the model overpredicts the number of low-mass stars, and the number of stars drops below $[Fe/H] < -5.07$, as shown in Figure 13. In addition, the predicted median of [C/Fe] is ~0 in this metallicity range.

Our results do not necessarily reject the possibility of fitting the abundance distributions of HMP/UMP stars in the framework of the faint-SN scenario. It is possible that the IMF is dependent on both the carbon and iron abundances, and we can construct such an abundance-dependent IMF that can reproduce the observed abundance distribution. However, it requires an extremely inefficient metal mixing in combination with the fine-tuning of the low-mass star formation rate for HMP/UMP stars. Even after accepting the difficulty, CEMP-no stars in Group I are still difficult to reproduce. A possible way to support the faint-SN scenario will be an SN-triggered star formation (Tsujimoto et al. 1999). If the second-generation low-mass stars are formed in the gas shell swept up by the ejecta of faint SNe, both the abundances and frequency of HMP/UMP stars may be reproduced, although we do not have a reliable model for the SN-triggered star formation. There are no predictions for the IMF of the second-generation stars in this model or the possibility of this star formation channel. These theoretical uncertainties involve the argument of the definition and the choice of model parameters and may encounter the same problem of the fine-tuning of free parameters. In addition, we need to explain the scarcity of CEMP-*s* stars for $[Fe/H] < -3.5$, the origin of which is attributed to the mass transfer from AGB stars to low-mass stars in the binary systems.

4. Binary Scenario

As an alternative scenario for the CEMP-no stars, we examine the binary scenario in which a mass transfer from AGB stars is responsible (Suda et al. 2004; Komiya et al. 2007).

We adopt the same assumptions for binary parameters as in Komiya et al. (2007). We apply the Bondi–Hoyle accretion for the stellar wind, which blows with the velocity of 20 km s^{-1} from AGB stars whose surface carbon abundance has been enhanced to $[C/H] = 0$. The accreted matter is mixed in the surface convection zone with the depth of 0.2 $M_\odot$.

The lognormal period distribution function is adopted, where the peak of the distribution is at $P = 10^{4.8}$ days with the dispersion of $\sigma_P = 2.3$, which is applicable to low-mass stars in the solar neighborhood (Duquennoy & Mayor 1991). Observationally, however, it is known that the fraction of CEMP-*s* stars drops below $[Fe/H] \sim -3$. This is indicative that the binary properties of lower-metallicity stars are different from more metal-rich stars, since the progress of *s*-process nucleosynthesis depends less on the metallicity for $[Fe/H] \lesssim -2$ (S. Yamada et al. 2020a, in preparation). We treat P and σ_P as free parameters and search for the values that can reproduce the observations.

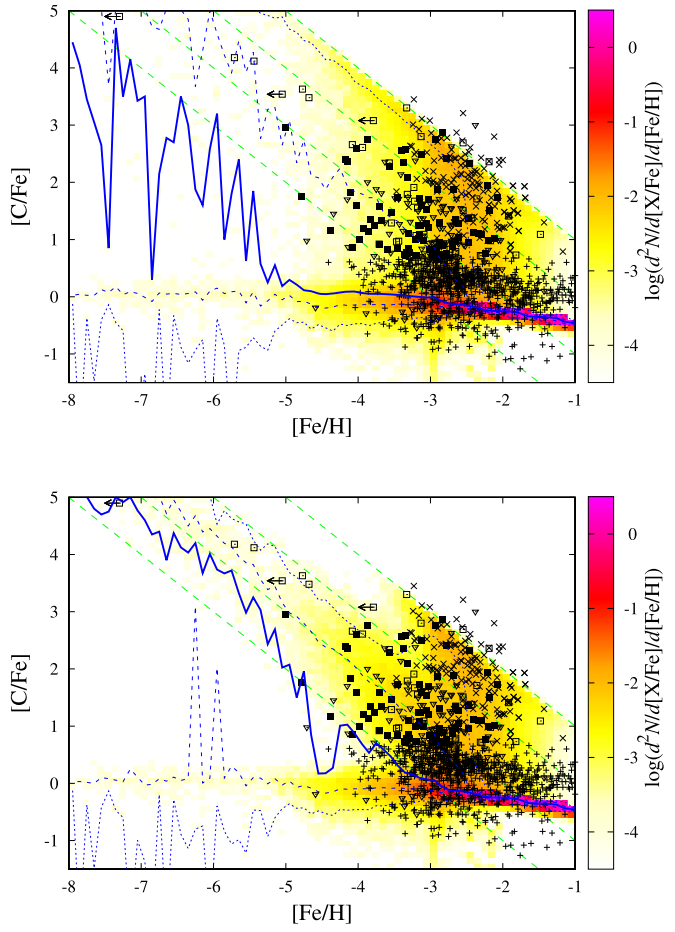

Figure 17. Distribution of carbon enhancement for the surface pollution by the binary mass transfer and the ISM accretion. We adopt the same period distribution of binaries as the Population I stars for the entire metallicity range (top panel) and the model with the period distribution of $P = 10^{4.5}$ days and $\sigma = 0.5$ at [Z/H] < -3 (bottom panel). In these models, faint SNe are not considered.

We take into account the surface pollution by the accretion of ISM here, which is neglected in the previous sections. It has been considered as the main origin of iron on CRUMP stars in the binary scenario (Suda et al. 2004; Komiya et al. 2015). In this case, CRUMP stars are formed in a Population III binary consisting of a low- or intermediate-mass primary star that can evolve to an AGB star and a low-mass secondary that can survive to date in the nuclear burning stages. The binary mass transfer changes the surface carbon abundance of the secondary but does not affect its iron abundance, while the ISM accretion changes its surface iron abundance.

Figure 17 shows the results for the binary mass transfer and the ISM accretion scenario. In the top panel, we assume the same period distribution for the entire metallicity range. The predicted abundance distribution is consistent with the observations for the metallicity of [Fe/H] $\gtrsim -3$. As discussed in previous studies, many CEMP-*s* stars are formed up to [C/H] $\simeq 0$ through the binary mass transfer from AGB stars. Since the mass transfer also takes place at [Fe/H] $\lesssim -3$, however, CEMP stars with [C/H] $\simeq 0$ are also formed at a lower metallicity range.

The Group I CEMP stars, not only CEMP-*s* stars but also CEMP-no stars with [C/H] $\gtrsim -1$, are very rare at [Fe/H] $\lesssim -3.5$, which implies the lack of short-period binaries that trigger the efficient mass transfer. In the bottom panel of Figure 17, we show the model with the optimum parameter set, $P = 10^{4.5}$ days and $\sigma_P = 0.5$, of the period distribution for the binaries in the low metallicity range of [Z/H] < -3. The majority of the HMP/UMP stars become CEMP stars with $-2 <$ [C/H] < -1 by the binary mass transfer, which is consistent with the observed CRUMP stars. It is to be noted that all the stars are assumed to be formed in binaries at [Z/H] < -3. HMP stars without carbon enhancement are possible. They are born with massive primary stars or belong to the binaries consisting of two low-mass stars that have not yet evolved to the AGB phase.

If the surface iron pollution by ISM accretion is not taken into account, the predicted MDF is the same as the model without faint SNe in Figure 6 because the binary mass transfer does not change the iron abundance. As mentioned in Section 3.1, the predicted MDF is almost consistent with the observations except that a significant number of Population III stars are expected to be observed instead of HMP/EMP stars.

The surface pollution by ISM accretion changes the surface metallicity of low-mass Population III stars up to [Fe/H] ~ -5 on average, which can be observed as HMP/UMP stars (Komiya et al. 2015; Shen et al. 2017). CEMP-no stars in Group I are formed in short-period binaries similar to CEMP-*s* stars but with the primary stars of $M \gtrsim 3.5\,M_\odot$ since they have a much smaller efficiency of *s*-process nucleosynthesis without the hydrogen ingestion by the helium flash convection as compared with CEMP-*s* stars with the primaries of $M < 3.5\,M_\odot$ (Suda et al. 2017; S. Yamada et al. 2020a, in preparation).

In summary, the binary mass transfer and the ISM accretion model with the change of binary period distribution at [Z/H] $= -3$ to -4 well reproduce the distribution of carbon abundances in all the subgroups of CEMP stars. This scenario is also consistent with the observed MDF including the absence of Population III stars.

5. Conclusions

We have investigated the origin of carbon-enhanced metal-poor stars with normal barium abundances (CEMP-no stars) using a chemical evolution model. We have updated the *StarTree* code, a chemical evolution model within the framework of the hierarchical galaxy formation, which is capable of tracing the inhomogeneous metal enrichment process inside protogalaxies. We consider two proposed scenarios for the origin of CEMP-no stars. One is the faint-SN scenario, in which first SN ejecta is rich in carbon relative to iron (or iron-poor) to produce CEMP-no stars. The other is the binary scenario, in which CEMP-no stars have accreted carbon-enhanced gas through the binary mass transfer from AGB companion stars.

We find that the faint-SN scenario for CEMP-no stars has severe difficulties in accounting for the abundance distribution of EMP stars. The predicted value of [C/H] for the second-generation stars is significantly lower than observed CRUMP stars, where most of HMP stars and UMP stars are distributed below [C/H] < -3. The discrepancies will be alleviated by decreasing both the swept-up mass by SNe and the diffusion coefficient of SN yields by an order of magnitude. However, the model with inefficient metal mixing results in the overproduction of HMP/UMP stars. Adopting the high star formation rate and the small mixing mass of SNe in combination with the

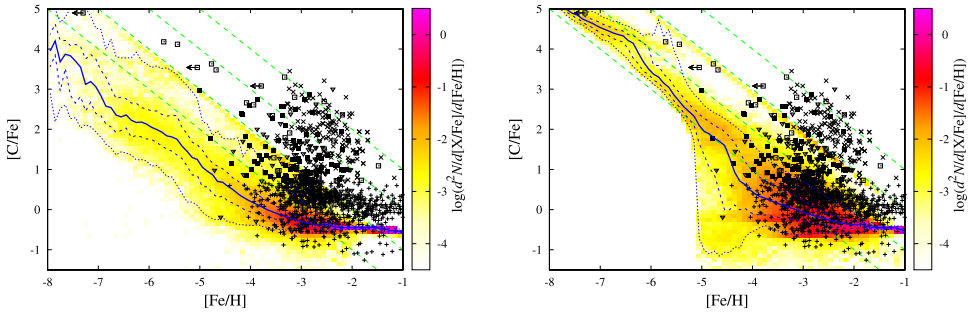

Figure 18. Results with the SN yields by Heger & Woosley (2010). The SN explosion energy ($E_{\rm SN}$) is (0.3–10) $\times$ 10^{51} erg. Left panel: result with the fiducial parameter set. Right panel: result with $C_{\rm diff} = 10^{-7}\,M_\odot\,{\rm yr}^{-3/2}$, $M_{\rm sw51} = 5.1 \times 10^3\,M_\odot$, and the low-mass star formation criterion by Chiaki et al. (2018b).

high-mass IMF of Population III stars, we can reproduce the scarcity of carbon-normal stars observed at [Fe/H] $\lesssim -4$. Another possibility to explain the high carbon abundance for HMP/UMP stars is the criterion for low-mass star formation depending on the carbon and iron abundances (Chiaki et al. 2018b). In these two models, however, the averaged [C/H] of HMP stars are lower than observed and the predicted number of UMP stars is significantly larger than observed.

A fine-tuning of the IMF at very low metallicity and extremely inefficient mixing of SN yields are demanded to explain the abundance distribution of HMP and UMP stars by the faint SN scenario. Even under these assumptions, a mechanism other than faint SNe is required for CEMP-no stars with large carbon enhancement of [C/H] > -1 in Group I defined by Yoon et al. (2016). It is only the Group II CEMP-no stars with weak carbon enhancement ([C/Fe] $\sim +1$) that can be naturally reproduced by the faint-SN models.

In contrast, the binary mass transfer scenario is able to well reproduce the observed distribution of carbon and iron abundances only if we assume the change of the period distribution below [Z/H] < -3. This is demanded from the observed scarcity of CEMP-*s* stars at [Fe/H] < -3.5.

If CEMP-no stars are formed through the binary mass transfer, they provide the information on the formation and evolution of binaries in the extremely low metallicity environment. Massive EMP or Population III binaries are discussed as possible progenitors of binary black holes, observed by the gravitational waves (e.g., Kinugawa et al. 2014). They can also become high-mass X-ray binaries and play an important role for the cosmic reionization (e.g., Ricotti & Ostriker 2004; Jeon et al. 2014). Detailed studies on the evolution of binary mass transfers in CEMP-no stars are expected to reveal the nature of binary systems under the extremely low metallicity.

We thank the anonymous referee for his/her useful comments and suggestions. This work has been partially supported by a Grant-in-Aid for Scientific Research (JP23224004, JP15HP7004, JP19HP8019, JP16K05287, JP16K05298, JP16H02168, JP19K-03931, and JP16H02166) from the Japan Society of the Promotion of Science.

Appendix
Supernova Yields

We test the SN yields by the "piston models" of Heger & Woosley (2010). In their models with some parameter sets, most of the iron falls back onto the central compact object while carbon-rich layers in the outer shells are ejected. The predicted yields give large [C/Fe] as in the mixing and fallback model associated with faint SNe.

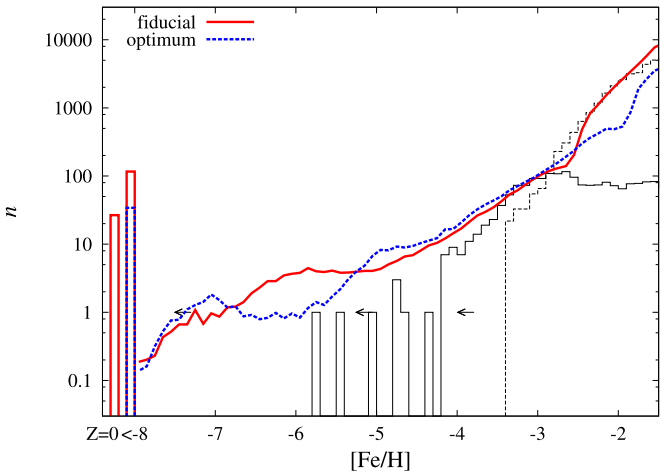

Figure 19. MDFs of the model with the SN yields of Heger & Woosley (2010). The red and blue lines denote the models in the left and right panels of Figure 18, respectively.

They provide Population III yields with various sets of progenitor mass, explosion energy, and mixing efficiency. We employ their S4 model with the mixing parameter set at zero. The explosion energy, $E_{\rm SN}$, is determined randomly from their 10 models as (0.3–10) $\times$ 10^{51} erg.

We adopt the yields for Population III stars by Heger & Woosley (2010) for [Z/H] < -3 and results of Woosley & Weaver (1995) at higher metallicity.

Some stars with $m \gtrsim 40\,M_\odot$ eject a large amount of carbon ($\Delta M_{\rm C} \gtrsim 1\,M_\odot$) in the models of Heger & Woosley (2010). These SNe can produce the second-generation stars with higher [C/H] than the fiducial model in Section 3. On the other hand, the majority of HMP/UMP stars also have [C/H] < -3 in the model with the fiducial parameter set, as shown in the left panel of Figure 18.

We tried to reproduce the distribution of observed abundances by tuning the parameters. The right panel of Figure 18 is one of the best-fit models. We adopt $C_{\rm diff} = 10^7\,M_\odot\,{\rm yr}^{-3/2}$, $M_{\rm sw51} = 5.1 \times 10^3$, and the low-mass star formation criterion by Chiaki et al. (2018b). In this case, we find an inconsistency with the observations as in the optimum case with the mixing and fallback models in Section 3.2.5. UMP stars are overproduced as shown in Figure 19, and the Group I stars are not reproduced as discussed.

ORCID iDs

Yutaka Komiya https://orcid.org/0000-0003-1555-7816
Takuma Suda https://orcid.org/0000-0002-4318-8715

References

Aoki, W., Beers, T. C., Christlieb, N., et al. 2007, ApJ, 655, 492
Arentsen, A., Starkenburg, E., Shetrone, M. D., et al. 2019, A&A, 621, A108
Beers, T. C., & Christlieb, N. 2005, ARA&A, 43, 531
Bessell, M. S., Collet, R., Keller, S. C., et al. 2015, ApJ, 806, 16
Carollo, D., Beers, T. C., Chiba, M., et al. 2010, ApJ, 712, 692
Carollo, D., Freeman, K., Beers, T. C., et al. 2014, ApJ, 788, 180
Chabrier, G. 2003, PASP, 115, 763
Chiaki, G., Susa, H., & Hirano, S. 2018a, MNRAS, 475, 4378
Chiaki, G., Tominaga, N., & Nozawa, T. 2018b, MNRAS, 472, 115
Cooke, R. J., & Madau, P. 2014, ApJ, 791, 116
Duquennoy, A., & Mayor, M. 1991, A&A, 248, 458
Hansen, T. T., Andersen, J., Nordström, B., et al. 2016, A&A, 586, A160
Heger, A. 2016, StarFit, http://starfit.org/
Heger, A., & Woosley, S. E. 2010, ApJ, 724, 341
Iwamoto, N., Umeda, H., Tominaga, N., Nomoto, N., & Maeda, K. 2005, Sci, 309, 451
Jeon, M., Pawlik, A. H., Bromm, V., & Milosavljević, M. 2014, MNRAS, 440, 3778
Karlsson, T. 2006, ApJL, 641, L41
Keller, S. C., Bessell, M. S., Frebel, A., et al. 2014, Natur, 506, 463
Kinugawa, T., Inayoshi, K., Hotokezaka, K., Nakauchi, D., & Nakamura, T. 2014, MNRAS, 442, 2963
Kobayashi, C., Umeda, H., Nomoto, K., Tominaga, N., & Ohkubo, T. 2006, ApJ, 653, 1145
Komiya, Y., Habe, A., Suda, T., & Fujimoto, Y. M. 2009a, ApJL, 696L, 79
Komiya, Y., Habe, A., Suda, T., & Fujimoto, Y. M. 2010, ApJ, 717, 542
Komiya, Y., & Shigeyama, T. 2016, ApJ, 830, 76
Komiya, Y., Suda, T., & Fujimoto, Y. M. 2009b, ApJ, 694, 1577
Komiya, Y., Suda, T., & Fujimoto, Y. M. 2015, ApJL, 808, L47
Komiya, Y., Suda, T., & Fujimoto, Y. M. 2016, ApJ, 820, 59
Komiya, Y., Suda, T., Minaguchi, H., et al. 2007, ApJ, 658, 367
Komiya, Y., Yamada, S., Suda, T., & Fujimoto, M. Y. 2014, ApJ, 783, 132
Lee, Y.-S., Suda, T., Beers, T. C., & Stancliffe, R. 2014, ApJ, 788, 131
Lucatello, S., Tsangarides, S., Beers, T. C., et al. 2005, ApJ, 625, 825
Machacek, M. E., Bryan, G. L., & Abel, T. 2001, ApJ, 548, 509
Maeder, A., Meynet, G., & Chiappini, C. 2015, A&A, 577, 56
Meynet, G., Ekstrom, S., & Maeder, A. 2006, A&A, 447, 623
Norris, J. E., Yong, D., Bessell, M. S., et al. 2013, ApJ, 762, 28
O'Shea, B. W., & Norman, M. L. 2008, ApJ, 673, 14
Parkinson, H., Cole, S., & Helly, J. 2007, MNRAS, 383, 557
Planck Collaboration, Ade, P. A. R., Aghanim, N., et al. 2016, A&A, 594, A13
Ricotti, M., & Ostriker, J. P. 2004, MNRAS, 352, 547
Rossi, S., Beers, T. C., & Sneden, C. 1999, ASPC, 165, 264
Sarmento, R., Scannapieco, E., & Pan, L. 2017, ApJ, 834, 23
Schaerer, D. 2002, A&A, 382, 28
Sharma, M., Theuns, T., Frenk, C. S., & Cooke, R. J. 2016, MNRAS, 473, 984
Shen, S., Kulkarni, G., Madau, P., & Mayer, L. 2017, MNRAS, 469, 4012
Sheth, R. K., Mo, H. J., & Tormen, G. 2001, MNRAS, 323, 1
Sheth, R. K., & Tormen, G. 2002, MNRAS, 349, 1464
Shigeyama, T., & Tsujimoto, T. 1998, ApJ, 507, 135
Shigeyama, T., Tsujimoto, T., & Yoshii, Y. 2003, ApJL, 586, L57
Smith, B. D., Wise, J. H., O'Shea, B. W., Norman, M. L., & Khochfar, S. 2015, MNRAS, 452, 2822
Somerville, R. S., & Kolatt, T. S. 1999, MNRAS, 305, 1
Starkenburg, E., Shetrone, M. D., McConnachie, A. W., & Venn, K. A. 2014, MNRAS, 441, 1217
Suda, T., Aikawa, M., Machida, M. N., Fujimoto, M. Y., & Iben, I., Jr. 2004, ApJ, 611, 476
Suda, T., Hidaka, J., Aoki, W., et al. 2017, PASJ, 69, 76
Suda, T., Katsuta, Y., Yamada, S., et al. 2008, PASJ, 60, 1159
Suda, T., Komiya, Y., Yamada, S., et al. 2013, MNRAS, 432, L46
Suda, T., Yamada, S., & Fujimoto, M. Y. 2017, JPSCP, 14, 010901
Suda, T., Yamada, S., Katsuta, Y., et al. 2011, MNRAS, 412, 843
Tominaga, N., Iwamoto, N., & Nomoto, K. 2013, ApJ, 785, 98
Tsujimoto, T., Shigeyama, T., & Yoshii, Y. 1999, ApJL, 519, L63
Umeda, H., & Nomoto, K. 2002, ApJ, 565, 385
Umeda, H., & Nomoto, K. 2005a, ApJ, 619, 427
Umeda, H., & Nomoto, K. 2005b, Natur, 422, 871
Woosley, S. E., & Weaver, T. A. 1995, ApJS, 101, 181
Yamada, S., Suda, T., Komiya, Y., Aoki, W., & Fujimoto, M. Y. 2013, MNRAS, 436, 1362
Yoon, J., Beers, T. C., Placco, V. M., et al. 2016, ApJ, 833, 20
Zhang, J., Fakhouri, O., & Ma, C.-P. 2008, MNRAS, 389, 1521